J. Chem. Thermodynamics 58 (2013) 166–195

Contents lists available at SciVerse ScienceDirect

J. Chem. Thermodynamics

journal homepage: www.elsevier.com/locate/jct

Al–Mg–RE (RE = La, Ce, Pr, Nd, Sm) systems: Thermodynamic evaluations and optimizations coupled with key experiments and Miedema's model estimations

Liling Jin [a,*], Dmytro Kevorkov [b], Mamoun Medraj [b], Patrice Chartrand [a]

[a] Centre de Recherche en Calcul Thermochimique (CRCT), Département de génie chimique, École Polytechnique, Montréal, QC, Canada H3C 3A7
[b] Department of Mechanical Engineering, Concordia University, Montréal, QC, Canada

ARTICLE INFO

Article history:
Received 20 July 2012
Received in revised form 17 September 2012
Accepted 24 October 2012
Available online 22 November 2012

Keywords:
Thermodynamics
Aluminium–magnesium–rare earth alloys
Modified Quasichemical Model
Electron probe micro-analysis

ABSTRACT

The solid solubilities of Al in $Mg_{12}La$, $Mg_{12}Ce$, $Mg_{12}Pr$, $Mg_{41}Nd_5$ phases were investigated by key experiments. The enthalpy of formation of ternary compounds was estimated using the model of Miedema. The systematic thermodynamic evaluation and optimizations of ternary Al–Mg–RE (RE = La, Ce, Pr, Nd, Sm) systems were based on the available experimental data and current investigation. The Al–Mg–Pr and Al–Mg–Nd systems were optimized for the first time using a systematic approach. Arc-melted key alloys were annealed at $T = 673$ K for four weeks and the phases were analyzed with electron probe micro-analysis (EPMA). The $Mg_{12}La$ intermetallic phase was confirmed by the present investigation. Optimized model parameters have been obtained for the Gibbs energy functions of all stable phases, and the model reproduces most critically assessed experimental results. The Modified Quasichemical Model, which takes short–range ordering into account, is used for the liquid phase and the Compound Energy Formalism (CEF) is used for the solid solutions in the binary and ternary systems. Kohler–type extrapolation from binary systems was employed, where no ternary parameters were used for the liquid phase.

1. Introduction

Magnesium–aluminium-based alloys are widely used because of their low density, high strength-to-weight ratio, specific rigidity, satisfactory salt-spray corrosion resistance and good ductility [1]. Special automobile applications, like engine blocks or power train components require sufficient creep resistance at elevated temperature. Lanthanum and cerium are two dominating constituents of the mischmetal, which is a mixture of rare earth elements (mostly light rare earths) with typical composition ranges of La (25–34)%, Ce (48–55)%, Pr (4–7)% and Nd (11–17)% [2]. These elements are important alloying additives for the development of magnesium alloys since adding rare earth (RE = La, Ce, Pr, Nd, Sm, Gd, Tb, Dy, Ho, Er, Tm, Lu, Y, and Sc) elements in Mg–Al alloys improve the creep resistance [3] and strength at elevated temperatures. This is attributed to the precipitation of intermetallic phases (such as $Al_{11}RE_3$ and Al_2RE phases), and the suppression of the formation of the detrimental $Mg_{17}Al_{12}$ phase in the interdendritic or grain boundary region. To estimate the nature of precipitating phases, precipitation sequences and the relative amounts of secondary phases, it is necessary to know thermodynamic properties and the phase diagram of the ternary Al–Mg–RE systems which requires a self-consistent thermodynamic database of Mg alloys containing rare earth elements.

Furthermore, it is worth noting the importance of the solid solubility of rare-earth metals in solid (Mg)-HCP phase in the multicomponent alloy systems, including the influence of Al, because of the positive effect of this solubility on the mechanical properties and plasticity of magnesium alloys. It was confirmed from the recent study of Hantzsche *et al.* [4] that magnesium sheets with weak textures, which promise improved sheet formability [5], can be obtained by adding alloying elements such as Nd, Ce and Y. It was also pointed out that the amount of the RE addition required for sufficient texture weakening depends on the solid solubility of the respective element in magnesium matrix.

Generally, phase equilibria and thermodynamic properties in the systems of the rare earth elements show smooth and regular variations when passing from one rare earth element to the next along the lanthanidelight rare earth series. Similarities among all the Mg–Al–RE ternary systems are also expected. As a matter of fact, the similar thermodynamic properties between the Al–Mg–RE (RE = Gd, Dy, Ho, Er) systems were already reported [6,7]. The Al–Mg–La, Al–Mg–Ce and Al–Mg–Sm ternary systems were optimized independently by Hosseinifar and Malakhov [8], Gröbner *et al.* [9] and Jia *et al.* [10], respectively. No thermodynamic optimization on the Al–Mg–Pr or Al–Mg–Nd system could be found in the literature. De Negri *et al.* [11] performed experimental investigation on Al–Mg–RE (RE = Gd, Dy, Ho) systems by differential thermal analysis (DTA), X-ray powder diffraction (XRD), light optical microscopy (LOM), scanning electron microscopy (SEM) and electron probe microanalysis (EPMA). Cacciamani *et al.* [6] did

* Corresponding author. Tel.: +1 514 3404711x2483; fax: +1 514 3405840.
E-mail address: liling.jin@polymtl.ca (L. Jin).

0021-9614/$ - see front matter © 2012 Elsevier Ltd. All rights reserved.
http://dx.doi.org/10.1016/j.jct.2012.10.021

thermodynamic modelling and optimization of Al–Mg–RE (RE = Gd, Dy, Ho) systems in a systematic manner based on the experimental information of De Negri *et al.* [11]. Saccone *et al.* [12] investigated experimentally the Al–Mg–Er ternary system using the same technique as those of De Negri *et al.* [11] while Cacciamani *et al.* [7] did thermodynamic modelling and optimization of Al–Mg–Er system. It is of great importance to study the Al–Mg–RE (RE = La, Ce, Pr, Nd, Sm) ternary systems in a systematic and consistent way especially as estimation techniques must be used for the mixing properties of intermetallic solutions. Furthermore, the systematic thermodynamic evaluations and modelling of Al–Mg–heavy RE (heavy RE = Gd, Tb, Dy, Ho, Er) systems were performed and presented in the dissertation of Jin [13].

As part of ongoing projects in our laboratory to develop thermodynamic databases for multi-component Mg- and Al-based alloys, the Al–Mg–light RE (La, Ce, Pr, Nd and Sm) were systematically evaluated and optimized based on (1) binary Al–Mg [14], Al–RE [15] and Mg–RE [16] thermodynamic and phase equilibria optimizations, (2) a critical literature review, (3) new experimental results from this work and (4) estimations from the model of Miedema carried out in the present study. Key experiments were performed to verify the phase relationship and solid solubility limits in the ternary systems. The binary Al–RE systems have been assessed previously by our group [15,17,18]. The trends in the thermodynamic properties (such as the enthalpy of mixing for the liquid, the entropy of mixing for the liquid, and the enthalpy of formation for the intermetallic compounds) of Al–RE systems were also discussed in Jin *et al.* [15,18].The binary thermodynamic parameters of Al-light RE (light RE = La, Ce, Pr, Nd, Sm) were taken from Jin *et al.* [15],where as the Mg-light RE binary systems were from Kang *et al.* [19].

2. Experimental information in the literature

For the Mg–Al–La system, Rogl [20]reported the experimental information published prior to the year 1988, while Raghavan [21] reviewed the experimental investigations published up to the year 2008. Zarechnyuk *et al.* [22] studied the partial isothermal section at 400 °C for La concentration up to 33.3 at.%. According to these authors, no ternary intermetallic compound was found and a limited solubility of Al in La_2Mg_{17} and in $LaMg_3$ was reported. Odinaev *et al.* [23] prepared 115 alloys with an arc melting furnace using Al, Mg, and Laas starting materials with 99.995, 99.95 and 98.48 wt.% purity, respectively. They annealed the alloys at 400 °C for 480 h. Phase equilibria in this isothermal section were then investigated by metallography and X–ray powder diffraction (XRD). Extensive solid solutions were observed. It was reported that $LaMg_2$ (prototype: $MgCu_2$) and $LaAl_2$ (prototype: $MgCu_2$) formed a continuous Laves_C15 solid solution at 673 K with a miscibility gap (20–37 at.% Mg) and LaMg (prototype: CsCl) formed an extensive BCC_B2 solid solution with LaAl (prototype: CeAl) up to ~29 at.% Al. Moreover, a ternary compound $Al_2Mg_{0.85}La_{0.15}$ of unknown structure was found to be stable at this temperature. Odinaev *et al.* [24] studied the phase equilibria in the Al–Mg–$LaAl_2$sub-system by metallography, DTA, and XRD. The liquidus projection and four pseudo-binary sections were constructed in this region. The existence of $LaMg_{12}$ phase remained unclear according to Raghavan [21], although the $LaMg_{12}$ phase was considered in the thermodynamic optimization of the La–Mg system by Guo and Du [25] based on the investigation of Darriet *et al.* [26]. Zheng *et al.* [27] investigated the liquidus surface in the Al-rich corner of the Al–Mg–La system and reported a eutectic reaction Liquid $\leftrightarrow \alpha Al_{11}La_3 + Al_3Mg_2 + Al$ at $T = 718$ K. Noting that Odinaev *et al.* investigated the Al–La–Mg [23], and Al–Ce–Mg [28] systems using the same experimental technique (DTA) to determine the liquidus temperatures and that the experimental work from Gröbner *et al.* [9] suggested the liquidus temperatures in the Al–Ce–Mg system were much higher than those from Odinaev *et al.* [28], Hosseinifar and Malakhov [8] recently studied two key alloys in the Al–Mg–La system (Al 60 wt.%, La 20.1 wt.%, Mg 19.9 wt.% and Al 70 wt.%, La 15.07 wt.%, Mg 14.93 wt.% respectively), by differential scanning calorimeter (DSC) to verify the liquidus temperatures and thermal arrests during the solidification process. They also reported an optimized Al–Mg–La ternary system.

For the Mg–Al–Ce system, Zarechnyuk and Kripyakevich [29] prepared 16 binary and 57 ternary alloys and determined a partial isothermal section at 673 K for Ce compositions up to 33.3 at.%. A ternary compound $Al_{67}Ce_5Mg_{28}$ was reported with a structure of the $MgZn_2$ type (hexagonal Laves_C14 phase with $a = 0.552$ nm and $c = 0.889$ nm). Two ternary compounds, $Al_{23}CeMg_9$ and Al_4CeMg_4 were reported by Cui and Wu [30] from their metallographic analysis on sixty arc-melted samples, which were annealed at $T = 673$ K for 608 h. The crystal structure of these two ternary compounds was not reported. However, these two compounds were not confirmed in a later study by Odinaev *et al.* [28] who reported a ternary compound $Al_2Ce_{0.2}Mg_{0.8}$ with the $MgZn_2$ type structure. This compound was most likely the same compound observed by Zarechnyuk and Kripyakevich [29]. In a later investigation, the same authors [31], using DTA, examined a number of pseudo–binary sections in the Al–Mg–Ce ternary system. It was reported that the ternary compound $Al_2Ce_{0.2}Mg_{0.8}$ (or $Al_2Ce_{0.15}Mg_{0.85}$) melts congruently at $T = 908$ K. Extensive solid solutions were observed by Odinaev *et al.* [28] based on microstructural and X–ray examinations. They reported that $CeMg_2$ and $CeAl_2$ form a continuous solid solution at $T = 673$ K with a miscibility gap (5–20 at.% Mg) and CeMg forms an extensive solid solution with CeAl up to ~30 at.% Al. Moreover, a limited solubility of Al in $CeMg_{12}$ was found [29]. Zheng *et al.* [32] measured a eutectic temperature at 719 K involving liquid–Al–$Al_{11}Ce_3$–$Al_{140}Mg_{89}$ by thermal analysis.

Recently, Gröbner *et al.* [9] prepared four key experiments by arc melting under purified argon, sealed them in silica tubes and annealed them at $T = 673$ K for 500 hours. According to their DTA and XRD studies, Gröbner *et al.* [9] suggested that the ternary compound $Al_{13}CeMg_6$ (referred to $Al_{67}Ce_5Mg_{28}$ [29], $Al_2Ce_{0.2}Mg_{0.8}$ or $Al_2Ce_{0.15}Mg_{0.85}$ [28,31]) melted incongruently around $T = 728$ K. It was also claimed that solid solutions of the BCC_B2, Laves_C15, and $Ce(Mg,Al)_{12}$ phases were formed in the Al–Mg–Ce ternary system and an optimized Al–Mg–Ce ternary system was obtained [9].

For the Al–Mg–Pr ternary system, no optimized ternary phase diagram could be found in the literature. This ternary system has been reviewed by Raghavan [33]. Odinaev *et al.* [34] prepared about 150 alloys with arc melting furnace and annealed them at $T = 673$ K for 480 hours with the starting metals of 99.995% Al, 99.95% Mg and 99.78% Pr. Phase equilibria in this isothermal section were investigated by metallography and XRD techniques. Extensive solid solutions were observed. They found that $PrMg_2$ (prototype: $MgCu_2$) and $PrAl_2$ (prototype: $MgCu_2$) form a continuous Laves_C15 solid solution at $T = 673$ K with a miscibility gap (5–27 at.% Mg), and PrMg (prototype: CsCl) forms an extensive BCC_B2 solid solution with PrAl up to ~30 at.% Al. Also, a ternary compound $Al_2Mg_{0.88}Pr_{0.12}$ of $MgZn_2$-type structure (Laves_C14) was found to be stable at this temperature. Odinaev *et al.* [35] prepared 153 alloys in the Al–Mg–$PrAl_2$ region with the same starting metals as used in their previous paper [34]. Phase equilibria were studied by metallography, DTA, and XRD techniques. The liquidus projection and four pseudo-binary sections were constructed in this region.

For the Mg–Al–Nd system, no optimized ternary phase diagram could be found in the literature. The Al–Mg–Nd ternary system has been reviewed by Raghavan [36]. Zarechnyuk *et al.* [22] studied a

TABLE 1
The solid phases in the Al–Mg–RE (RE = La, Ce, Pr, Nd, Sm) systems.

Phase symbol	Phase description	Prototype	Pearson symbol
BCC_B2	(Mg, Al)(Mg, La, Ce, Pr, Nd, Sm)	CsCl	cP2
Laves_C15	(Mg, Al, La, Ce, Pr, Nd, Sm)$_2$(Mg, Al, La, Ce, Pr, Nd, Sm)	Cu_2Mg	cF24
Mg3RE	(Mg, Al)$_3$(Mg, La, Ce, Pr, Nd, Sm)	BiF_3	cF16
Al3RE	(Mg, Al)$_3$(La, Ce, Pr, Nd, Sm)	Ni_3Sn	hP8
Al11RE3	(Mg, Al)$_{11}$(La, Ce, Pr, Nd, Sm)$_3$	αLa_3Al_{11}	oI28
Mg12RE	(Mg, Al)$_{12}$(La, Ce, Pr, Nd, Sm)	$CeMg_{12}$	oI338
Mg41RE5	(Mg, Al)$_{41}$(La, Ce, Pr, Nd, Sm)$_5$	$Mg_{41}Ce_5$	tI92
Mg17RE2	(Mg, Al)$_{17}$(La, Ce, Pr, Nd, Sm)$_2$	$Ni_{17}Th_2$	hP38
BCC_A2	(Al, Mg, La, Ce, Pr, Nd, Sm)	W	cI2
FCC_A1	(Al, Mg, La, Ce, Pr, Nd, Sm)	Cu	cF4
HCP_A3	(Al, Mg, La, Ce, Pr, Nd, Sm)	Mg	hP2
DHCP_A3′	(Al, Mg, La, Ce, Pr, Nd, Sm)	La	hP4
Gamma	(Mg)$_{10}$(Mg, Al)$_{24}$(Mg, Al)$_{24}$	αMn	cI58
Beta	(Al)$_{19}$(Mg,Al)$_2$(Mg)$_{12}$		
$Al_{30}Mg_{23}$	Stoichiometric		
$La_{22}Al_{53}$	Stoichiometric	AlB_2	hP3
LaAl	Stoichiometric	AlCe	oC16
CeAl	Stoichiometric	AlCe	oC16
Ce_2Al	Stoichiometric		
αCe_3Al	Stoichiometric	Ni_3Sn	hP8
βCe_3Al	Stoichiometric	$AuCu_3$	cP4
αPr_3Al	Stoichiometric	Ni_3Sn	hP8
βPr_3Al	Stoichiometric	$AuCu_3$	cP4
Pr_2Al	Stoichiometric	Co_2Si	oP12
PrAl	Stoichiometric	ErAl	oP16
NdAl	Stoichiometric	ErAl	oP16
Nd_2Al	Stoichiometric	Co_2Si	oP12
Nd_3Al	Stoichiometric	Ni_3Sn	hP8
Sm_2Al	Stoichiometric	Co_2Si	oP12
SmAl	Stoichiometric	ErAl	oP16
$Al_{40}Mg_{17}La_3$	Stoichiometric		
$Al_{13}Mg_6Ce$	Stoichiometric	$MgZn_2$	*hP*12
$Al_{50}Mg_{22}Pr_3$	Stoichiometric	$MgZn_2$	*hP*12
$Al_{50}Mg_{22}Nd_3$	Stoichiometric	$MgZn_2$	*hP*12

TABLE 2
The enthalpies of formation of several Al–RE, Mg–RE and Al–Mg–RE compounds calculated by the Miedema's model.

Compounds	$\Delta_f H^o$/(kJ·mol^{-1} of atoms)
$Al_{12}La$	−11.70
$Al_{12}Ce$	−11.39
$Al_{12}Pr$	−11.30
$Al_{12}Nd$	−12.56
$Al_{12}Sm$	−11.18
$Al_{17}La_2$	−15.72
$Al_{17}Ce_2$	−15.41
$Al_{17}Pr_2$	−15.26
$Al_{17}Nd_2$	−16.98
$Al_{17}Sm_2$	−15.13
$Al_{41}La_5$	−16.20
$Al_{41}Ce_5$	−15.89
$Al_{41}Pr_5$	−15.73
$Al_{41}Nd_5$	−17.51
$Al_{41}Sm_5$	−15.61
$Mg_{11}La_3$	−4.10
$Mg_{11}Ce_3$	−5.21
$Mg_{11}Pr_3$	−5.07
$Mg_{11}Nd_3$	−5.92
$Mg_{11}Sm_3$	−5.06
$Al_2Mg_{0.8}Ce_{0.2}(Al_{13}Mg_6Ce)$	−12.67
$Al_2Mg_{0.85}La_{0.15}(Al_{40}Mg_{17}La_3)$	−10.49
$Al_2Mg_{0.88}Pr_{0.12}(Al_{50}Mg_{22}Pr_3)$	−7.60
$Al_2Mg_{0.88}Nd_{0.12}(Al_{50}Mg_{22}Nd_3)$	−8.35

partial isothermal section at 673 K for Nd composition up to 33.3 at.%. No ternary intermetallic compound was reported and a limited solubility of Al in $NdMg_{12}$ and in $NdMg_3$ was found. Odinaev *et al.* [37] prepared 87 alloys with arc melting furnace and annealed them at 673 K for 480 h with the starting metals of 99.995% Al, 99.95% Mg, and 99.98% Nd purity. Phase equilibria in this isothermal section were investigated by metallography and XRD techniques. Extensive solid solutions were also observed. According to their investigation [37], $NdMg_2$(prototype: $MgCu_2$) and $NdAl_2$(prototype: $MgCu_2$) form a continuous Laves_C15 solid solution at T = 673Kwith a miscibility gap (3–30 at.% Mg) and NdMg (prototype: CsCl) forms an extensive BCC_B2 solid solution with NdAl up to ~40 at.% Al. Also, a ternary compound $Al_2Mg_{0.88}Nd_{0.12}$ of $MgZn_2$-type structure (Laves_C14) was stable at this temperature. Odinaev *et al.* [38] prepared 60 alloys in the Al–Mg–$NdAl_2$ region with the same starting metals as used in their previous paper [37]. Phase equilibria were studied by metallography, DTA, and XRD techniques. The liquidus projection and several pseudo-binary sections were constructed in this region.

The Al–Mg–Sm ternary system has been reviewed by Raghavan [39]. Zheng *et al.* [40] reported 15 single phase regions, 27 two-phase regions, and 13 three-phase regions for the isothermal section at T = 673 K studied by X-ray, metallographic and chemical analysis, and no ternary compound was found. No experimental thermochemical data for this system are available in the literature. Jia *et al.* [10] optimized this ternary phase diagram based on the investigation by Zheng *et al.* [40]. No ternary interaction parameters were used and the ternary phase diagram was merely extrapolated from three binary sub-systems.

3. Methodology

3.1. Experimental methods

A solid–solid diffusion couple for the Al–Mg–La system was prepared from two blocks of Mg and Al alloys with a La foil in the middle, like a sandwich. The blocks' facing surfaces and the La foil were pre-ground up to 1200 grit using SiC paper and polished using 1 μm water-based diamond suspension. The blocks were pressed

together using a hydraulic press, placed in a Ta container and then sealed in a quartz tube under protective argon atmosphere. The prepared samples were annealed at T = 673 K for four weeks before quenching in cold water. The annealed samples were grinded and polished before being analyzed by electron probe microscopy analysis (EPMA) using point and line scans. However, no intermediate layers in the Al–Mg–La solid–solid diffusion couple were observed, probably due to the small diffusion coefficient at 673 K or poor surface contact. Therefore, two key samples were arc–melted in a water-cooled copper crucible under protective argon atmosphere in order to avoid extensive oxidation of Mg and Al. The starting materials are: La foil [50 mm ∗50 mm∗1.0 mm ,99.9 wt.% Rare Earth Oxide (REO) purity], Al ingot (99.999 wt.%) and Mg ingot (99.8 wt.%).

A solid–liquid diffusion couple in the Al–Mg–Ce system was prepared using $Mg_{0.667}Ce_{0.333}$and $Al_{0.667}Ce_{0.333}$ alloys. The block with lower liquidus temperature ($Mg_{0.667}Ce_{0.333}$ alloy) was melted on top of the block with higher melting temperature ($Al_{0.667}Ce_{0.333}$ alloy) in an arc-melting furnace. Furthermore two additional key samples of Al–Mg–Ce alloys were prepared. The prepared samples were also annealed at T = 673 K for four weeks. The annealed alloys were grinded and polished before EPMA analysis. The starting materials are: Ce ingot (99.8% (REO)), Al ingot (99.999 wt.%) and Mg ingot (99.8 wt.%).

Four ternary alloys in the Al–Mg–Pr system were prepared by melting stoichiometric amounts of the constituent elements in tantalum crucibles placed in an induction furnace under a protective argon atmosphere. Two alloys for the Al–Mg–Nd system were melted in an arc-melting furnace in a water-cooled copper crucible under a protective argon atmosphere. The prepared samples were annealed in a resistance furnace at 673 K for four weeks before quenching in cold water. All the samples were grinded up to 1200 grit using SiC paper and polished using 1 μm water-based diamond suspension. Electron probe microscopy analysis (EPMA)

TABLE 3
Composition and microanalysis data of the alloys studied.

Sample	Ternary system	Nominal alloy composition (at.%)	Observed phases	EPMA analysis (at.%)		
				Al	Mg	RE
A1	Al–Mg–La	$Al_{10}Mg_{82}La_8$	(Mg)	0.3	99.4	0.3
			$(Al_xMg_{1-x})_2La$	58.9	8.4	32.7
			$(Al_xMg_{1-x})_{12}La$	1.3	91.2	7.5
A2	Al–Mg–La	$Al_{80}Mg_{12.5}La_{7.5}$	$(Al_xMg_{1-x})_{11}La_3$	78.4	1.5	20.1
			(Al)	90.7	9.1	0.2
			Ternary phase τ1	69.0	23.9	7.1
A3	Al–Mg–Ce	$Al_{76}Mg_{16}Ce_8$	(Al)	89.4	10.5	0.1
			$(Al_xMg_{1-x})_{11}Ce_3$	77.4	0.3	22.3
			Ternary phase τ2	66.0	26.7	7.3
A4	Al–Mg–Ce	$Al_8Mg_{57}Ce_{35}$	$(Al_xMg_{1-x})Ce$	42.2	7.7	50.1
			$(Al_xMg_{1-x})_2Ce$	9.2	56.4	34.4
A5	Al–Mg–Pr	$Al_{10.6}Mg_{79.4}Pr_{10}$	(Mg)	0.0	99.9	0.1
			$(Al_xMg_{1-x})_2Pr$	61.0	4.8	34.2
			$(Al_xMg_{1-x})_{12}Pr$	0.3	91.9	7.8
A6	Al–Mg–Pr	$Al_{56.2}Mg_{22.4}Pr_{21.4}$	(Mg)	2.0	98.0	0.0
			$(Al_xMg_{1-x})_2Pr$	64.5	1.5	34.0
			$(Al_xMg_{1-x})_3Pr$	71.2	3.7	25.1
A7	Al–Mg–Pr	$Al_{34}Mg_{63}Pr_3$	(Mg)	8.6	91.4	0.0
			$(Al_xMg_{1-x})_{11}Pr_3$	73.6	3.3	23.1
			Gamma	37.3	60.9	1.8
A8	Al–Mg–Pr	$Al_{78}Mg_{15}Pr_7$	(Al)	92.2	7.8	0.0
			$(Al_xMg_{1-x})_{11}Pr_3$	76.2	0.2	23.6
			Ternary phase τ3	66.9	27.0	6.1
A9	Al–Mg–Nd	$Al_{26.9}Mg_{70.3}Nd_{2.8}$	(Mg)	10.3	89.6	0.1
			$(Al_xMg_{1-x})_{11}Nd_3$	76.1	1.8	22.1
			Gamma	38.3	60.5	1.2
A10	Al–Mg–Nd	$Al_{10.6}Mg_{79.4}Nd_{10}$	(Mg)	0.2	99.3	0.5
			$(Al_xMg_{1-x})_2Nd$	61.6	4.3	34.1
			$(Al_xMg_{1-x})_{41}Nd_5$	0.2	89.9	9.9

Note: The error of EPMA measurements is approximately ±2 at.%.

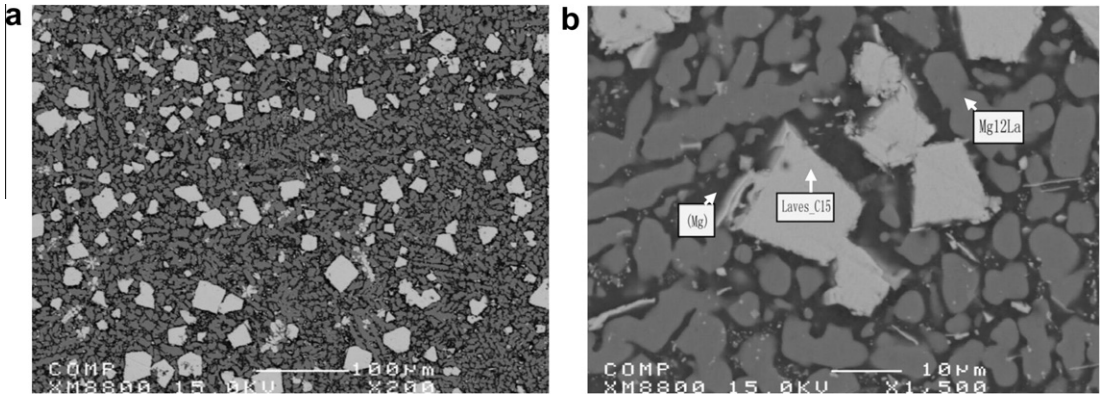

FIGURE 1. Backscattered electron images of $Al_{0.1}Mg_{0.82}La_{0.08}$ alloy annealed at T = 673 K for four weeks.

was employed to detect the phases and determine their compositions. The starting materials were: Pr ingot (99.9% (REO)), Nd ingot (99.8% (REO)), Al ingot (99.999 wt.%) and Mg ingot (99.8 wt.%).

It was noted that some magnesium and aluminium loss was observed during arc-melting process. To compensate for the mass loss of Mg and Al, additional 6 and 4 wt.% of Mg and Al, respectively, guided by trial and error method, were added into the nominal composition in order to investigate the desired phase equilibria. For the studies of phase equilibria in this work, it was judged unnecessary to get the actual compositions, which could be determined by inductively coupled plasma mass spectrometry (ICP-MS) method.

3.2. Miedema model estimations for binary and ternary thermodynamic data

The enthalpy of mixing [41,42] for an A–B disordered solution is estimated using the Miedema model with the following expression:

$$\Delta H_{AB} = f_{AB} \times \frac{x_A(1+\mu_A x_B(\phi_A-\phi_B))x_B(1+\mu_B x_A(\phi_B-\phi_A))}{x_A V_A^{2/3}[1+\mu_A x_B(\phi_A-\phi_B)]+x_B V_B^{2/3}[1+\mu_B x_A(\phi_B-\phi_A)]}. \quad (1)$$

For an ordered stoichiometric compound, enthalpy of formation is given by the following expression:

$$(\Delta H_{AB})_{\text{order}} = \Delta H_{AB} \times \left[1+\gamma\left(\frac{V_A^{1/3}V_B^{1/3}\Delta H_{AB}}{f_{AB}\{x_A V_A^{2/3}[1+\mu_A x_B(\varphi_A-\varphi_B)]+x_B V_B^{2/3}[1+\mu_B x_A(\varphi_B-\varphi_A)]\}}\right)^2\right], \quad (2)$$

$$f_{AB} = \frac{2PV_A^{2/3}V_B^{2/3}}{\frac{1}{n_{WS_A}^{1/3}}+\frac{1}{n_{WS_B}^{1/3}}}\cdot\left[-(\phi_B^*-\phi_A^*)^2+\frac{Q}{P}(n_{WS_A}^{1/3}-n_{WS_B}^{1/3})^2-a\times\frac{R}{P}\right]. \quad (3)$$

In equations (1)–(3), x_i, ϕ_i, V_i, n_{WS_i} are the mole fraction, chemical potential (or work function), molar volume, and the electronic density at the Wigner-Seitz cell boundary of component i, respectively. a, P, $\frac{R}{P}$, $\frac{Q}{P}$, μ_A, μ_B and γ are semi-empirical parameters evaluated and reported in Miedema [41]. The empirical parameter P assumes different values depending if A and B are both transition, both non-transition, or transition and non-transition elements; Q/P is assumed to be a constant that equals 9.4 [41].

The formation enthalpy of a crystalline solid solution can be described as [43]:

$$\Delta H^{\text{cryst}} = \Delta H^{\text{chem}} + \Delta H^{\text{elastic}} + \Delta H^{\text{struct}}, \quad (4)$$

where ΔH^{chem}: chemical contribution due to the mixing of two components given by equation (1); $\Delta H^{elastic}$: elastic contribution due to the atom-size mismatch effect; ΔH^{struct}: structural contribution due to the valence and crystal structure difference of the two components.

$$\Delta H^{\text{elastic}} = x_A \cdot x_B(x_A\Delta H_{\text{Bin}A}^{\text{elastic}} + x_B\Delta H_{\text{Ain}B}^{\text{elastic}}), \quad (5)$$

where $\Delta H_{\text{Bin}A}^{\text{elastic}}$ and $\Delta H_{\text{Ain}B}^{\text{elastic}}$ are the atom-size mismatch contribution to the solution enthalpy in a binary system. It can be evaluated by the following expression:

$$\Delta H_{\text{Ain}B}^{\text{elastic}} = \frac{2G_B(V_A^*-V_B^*)^2}{3V_B^*+4G_B K_A V_A^*}, \quad (6)$$

$$(V_i^*)^{2/3} = V_i^{2/3}(1+\mu_i(\varphi_i-\varphi_j)) \quad (i,j=A,B), \quad (7)$$

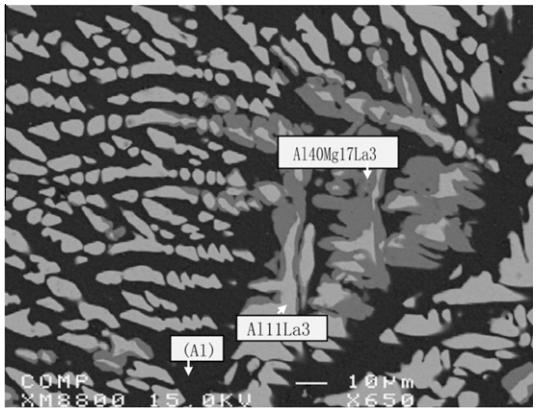

FIGURE 2. Backscattered electron images of $Al_{0.8}Mg_{0.125}La_{0.075}$ alloy annealed at T = 673 K for four weeks.

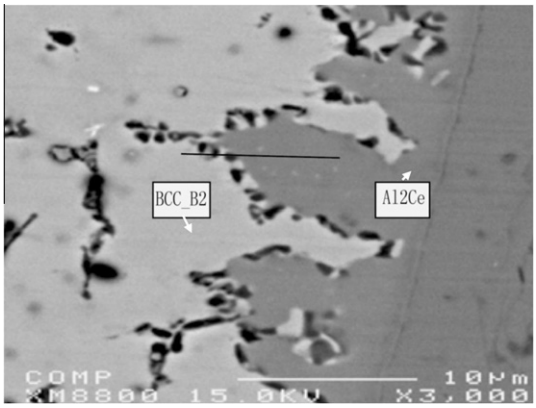

FIGURE 3. Backscattered electron image of the solid–solid Al_2Ce–$MgCe$ diffusion couple annealed at T = 673 K for 10 weeks.

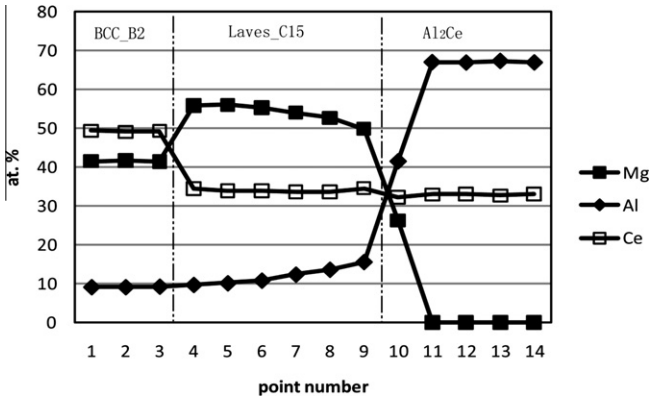

FIGURE 4. The composition profiles from the line scan of the Al_2Ce–Mg_2Ce diffusion couple (the error of EPMA measurements is approximately ±2 at.%).

where G_B is the shear modulus of the solvent; K_A is the compressibility of the solute and V_i^* (i = A, B) are the molar volumes of the solute or the solvent.

The structural contribution to the enthalpy is difficult to obtain without the use of *ab initio* calculations. It is argued that this contribution has a minor effect compared to the chemical and elastic contribution to the total enthalpy [44]. In the present study, the structural contribution is neglected.

$$\Delta H^{\text{struct}} \approx 0. \quad (8)$$

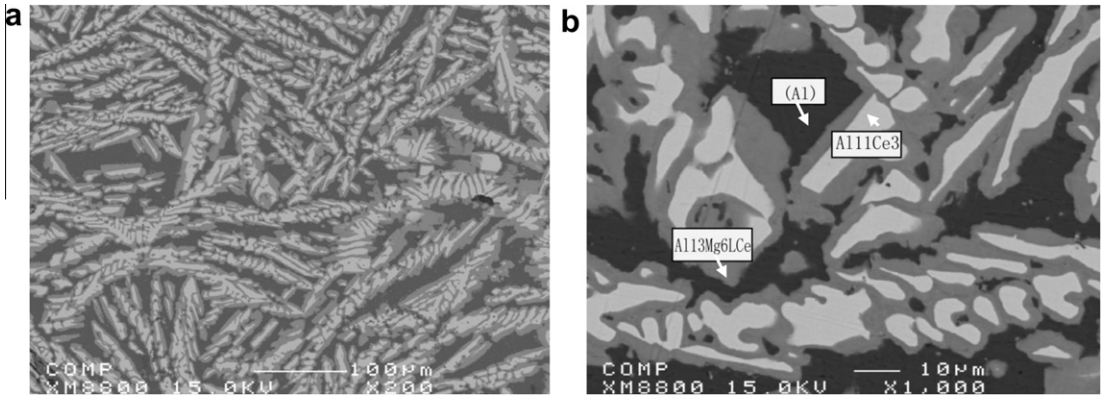

FIGURE 5. Backscattered electron images of the $Al_{0.76}Mg_{0.16}Ce_{0.08}$alloy annealed at T = 673 K for four weeks.

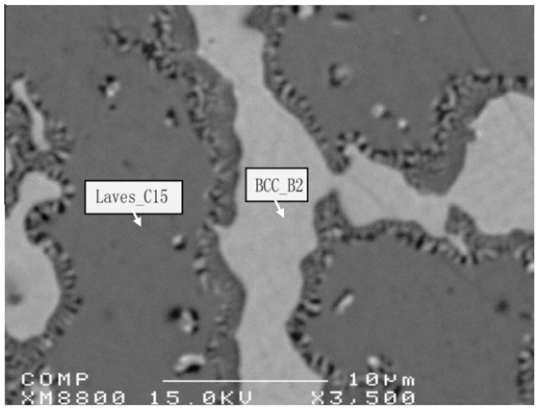

FIGURE 6. Backscattered electron images of the $Al_{0.08}Mg_{0.57}Ce_{0.35}$ alloy annealed at T = 673 K for four weeks.

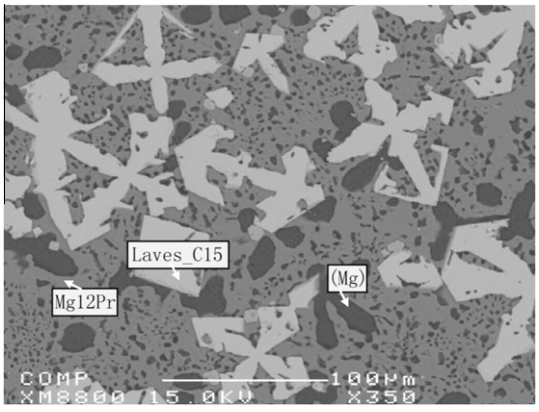

FIGURE 7. Backscattered electron images of the $Al_{0.106}Mg_{0.794}Pr_{0.10}$ alloy annealed at T = 673 K for four weeks.

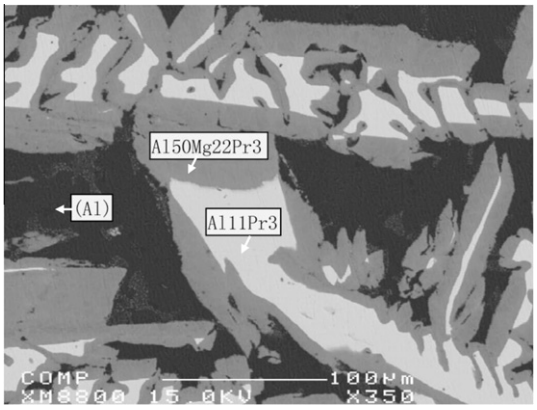

FIGURE 8. Backscattered electron images of the $Al_{0.78}Mg_{0.15}Pr_{0.07}$ alloy annealed at T = 673 K for four weeks.

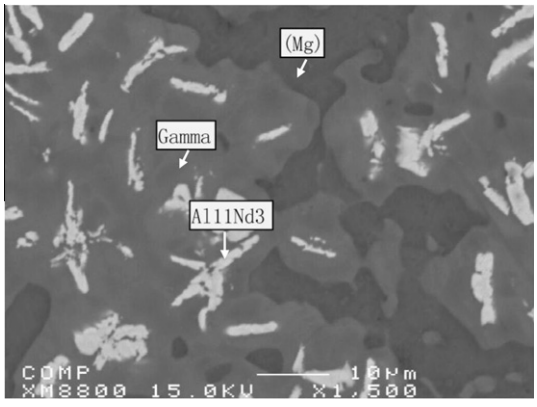

FIGURE 9. Backscattered electron images of the $Al_{0.269}Mg_{0.703}Nd_{0.028}$ alloy annealed at T = 673 K for four weeks.

The enthalpy of formation of a ternary alloy is assumed to be the sum of contribution from the three binary sub-systems. For a ternary system, there are a few simple and reliable interpolation models such as those of Kohler, Muggianu and Toop to estimate the thermodynamic properties from the binary sub-systems. A general interpolation technique of the thermodynamic model for the multicomponent systems is given by Pelton [45]. The choice of the interpolation model should be made according to the thermodynamic properties of the three sub-binary alloys. In the current study, the thermodynamic properties (like enthalpy of mixing in the liquid) of the three binary systems Al–Mg, Al–RE and Mg–RE are quite different from each other. The Kohler model is chosen in the present study, and the enthalpy of formation for the ternary compound can be expressed as:

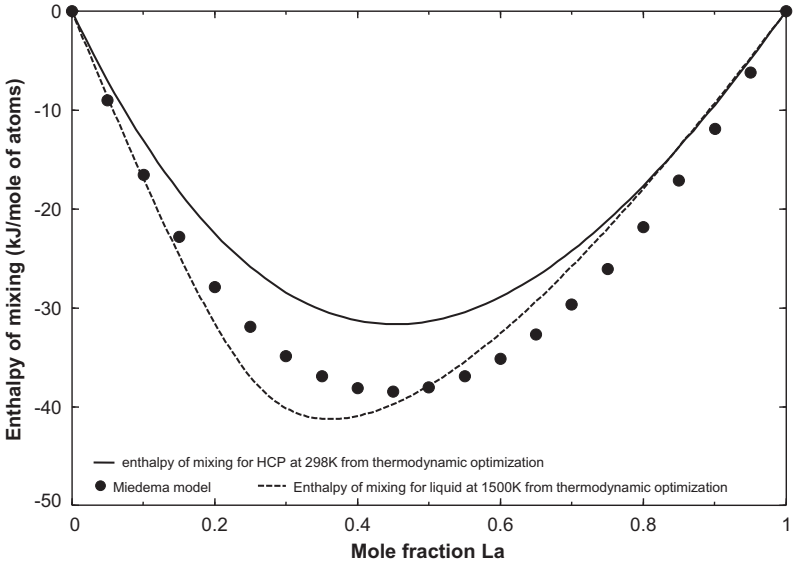

FIGURE 10. The enthalpy of mixing of the HCP solid solution in the Al–La system.

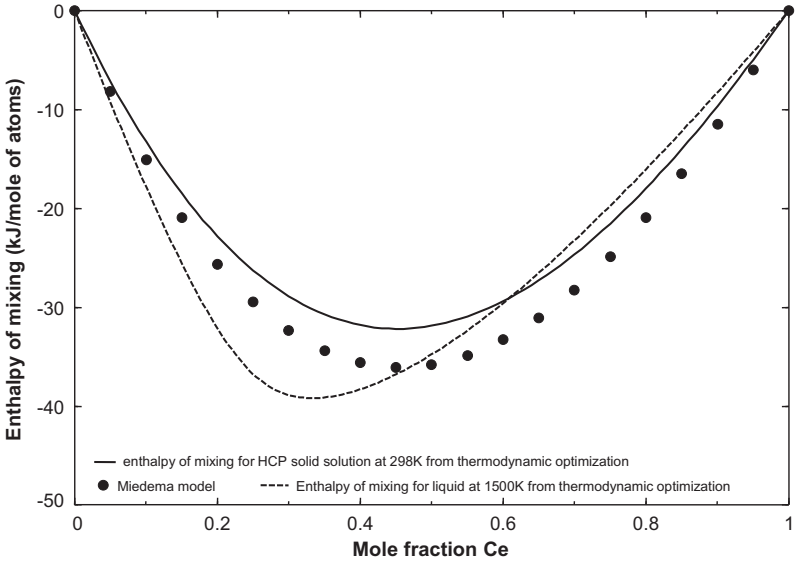

FIGURE 11. The enthalpy of mixing of the HCP solid solution in the Al–Ce system.

$$\Delta H_{ijk}^{\text{cryst}} = (1-x_i)\Delta H_{jk}^{\text{cryst}}\left(\frac{x_j}{x_j+x_k},\frac{x_k}{x_j+x_k}\right) + (1-x_j)\Delta H_{ik}^{\text{cryst}}\left(\frac{x_i}{x_i+x_k},\frac{x_k}{x_i+x_k}\right) + (1-x_k)\Delta H_{ij}^{\text{cryst}}\left(\frac{x_i}{x_i+x_j},\frac{x_j}{x_i+x_j}\right), \quad (9)$$

where i, j, k are the three components in a ternary system, x_i, x_j or x_k is the mole fraction of each component, $\Delta H_{ij}^{\text{cryst}}$, $\Delta H_{jk}^{\text{cryst}}$, $\Delta H_{ik}^{\text{cryst}}$ and $\Delta H_{ijk}^{\text{cryst}}$ are the contributions (chemical, elastic and structural contributions) of the three sub-binary systems and ternary system, respectively. The chemical and elastic enthalpies of ternary alloys can be extrapolated similarly from those of sub-binary systems by the equation (9).

The model parameters of ϕ_i, V_i, and n_{WS_i} from Shubin and Shunya'ev [46] were preferred in the present calculations. The estimations of the enthalpy of formation using the model parameters from Shubin and Shunya'ev [46] gives better agreement with the available experimental data than those calculated from the model parameters of Boer *et al.* [41].

3.3. Thermodynamic models used in the present study

All the present optimizations have been carried out using FactSage thermodynamic software [47]. The thermodynamic properties of pure Mg and light rare earth (La, Ce, Pr, Nd and Sm) are taken from the SGTE database [48], except the Pr and Sm in the FCC-structure, together with La, Pr, Nd and Sm in the HCP-structure which are taken from Kang *et al.* [16]. The present study is based on thermodynamic and phase equilibrium modelling of Al–Mg, Al–RE and Mg–RE (RE = La, Ce, Pr, Nd and Sm) binary systems [14–16], in which the Modified Quasichemical Model (MQM) was used for the liquid phase with a consistent set of coordination numbers for the elements ensuring compatibility with our previous database.

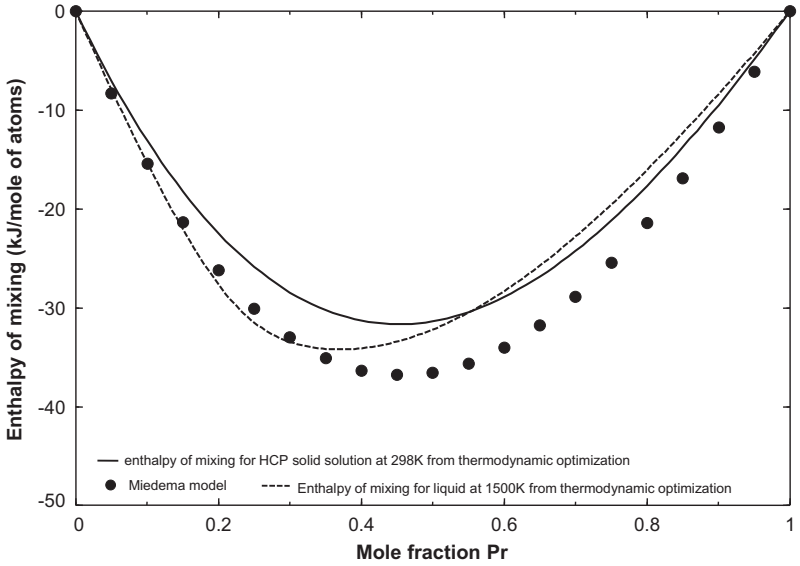

FIGURE 12. The enthalpy of mixing of the HCP solid solution in the Al–Pr system.

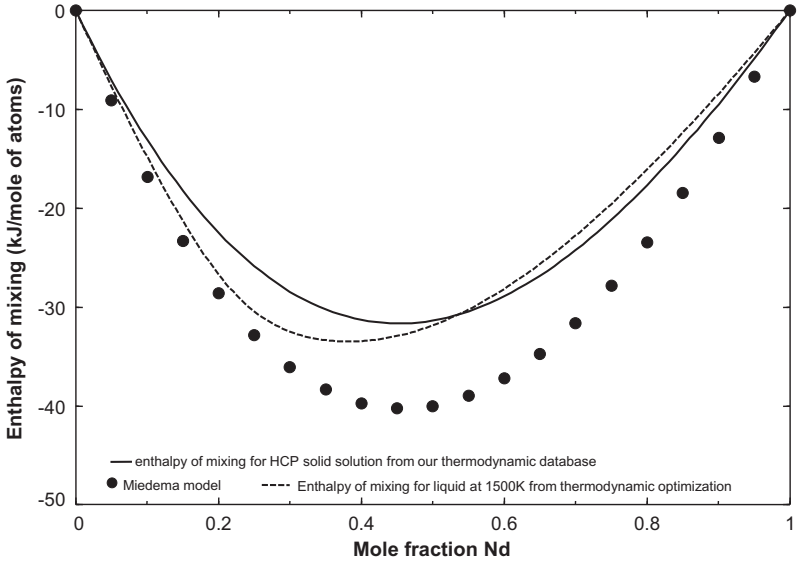

FIGURE 13. The enthalpy of mixing of the HCP solid solution in the Al–Nd system.

3.3.1. Modified Quasichemical Model (MQM) for the liquid phase

The detailed description of the MQM can be found in Pelton *et al.* [49]. A brief summary of MQM is given in Jin *et al.* [15,18]. The same notation is used in the present article. The MQM has been successfully applied to alloy liquid solutions [50,51], molten oxides [52,53], molten salts [54,55], and molten metal-sulphides systems [56]. As was shown by Kang *et al.* [51], liquid Mg–RE alloys usually exhibits a strong short-range ordering near $X_{RE} = 0.25$–0.33. Such short-range ordering in binary liquid alloy becomes more evident in several binary Al–RE systems as discussed by Jin *et al.* [15,18]. In order to treat short-range ordering effectively in the Mg–Al–RE ternary systems, the Modified Quasichemical Model in the pair approximation has been used in the present study. The Kohler-like method [45] was used to estimate the excess Gibbs energy in the ternary liquid in the present study.

3.3.2. Compound Energy Formalism (CEF) for solid solutions

The compound energy formalism [57–60] was introduced to describe the Gibbs energy of solid phases with sub–lattices. Ideal mixing of species on each sub-lattice is assumed. The sub-lattice stoichiometry depends on the base crystal structure. The same notation for the model parameters is used as those in Kang *et al.* [17].

Table 1 shows the reported crystal structures of the stable binary and ternary phases of the studied systems. In the present work, it is assumed that Mg and Al can potentially substitute each other on their respective sub-lattices for all solid solutions. As shown in table 1, the ternary phases ($Al_{40}Mg_{17}La_3$, $Al_{13}Mg_6Ce$, $Al_{50}Mg_{22}Pr_3$, and $Al_{50}Mg_{22}Nd_3$) are considered to be stoichiometric phases, although a narrow homogeneity range of their existence could not be excluded. The CEF is used for all solid solutions in the present study, and the sub-lattices species for each one is given in table 1. For each intermetallic phase in the Mg-light RE (MgRE, Mg_3RE, $Mg_{12}RE$, $Mg_{41}RE_5$, and $Mg_{17}RE_2$ phases) and Al-light RE (Al_2RE, Al_3RE, and $Al_{11}RE_3$ phases) sub-systems, a solid solution with the corresponding crystal structure is constructed, where a substitution of the RE elements by another light RE is permitted. For the Mg_3RE solid solution, the same model is used as the one from Kang *et al.*

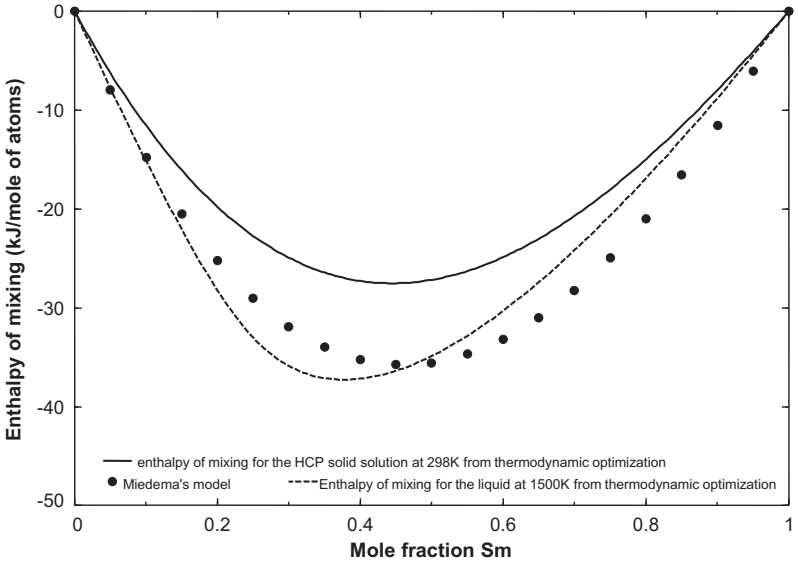

FIGURE 14. The enthalpy of mixing of the HCP solid solution in the Al–Sm system.

TABLE 4
Some invariant reactions of the Al–Mg–La system for $X_{La} < 1/3$.

Reaction	T/K		Type[a]	Composition/(at.%)			
	Exp.[b]	Calc.		Phase	Calc.		
					Al	La	Mg
L + $Al_{53}La_{22}$ ↔ Laves_C15 + $LaAl_3$		1468	U	L	73.0	23.9	3.1
L ↔ HCP + Laves_C15 + La(Mg,Al)$_{12}$		873	E	L	2.2	3.8	94.0
L ↔ FCC + $La_3Al_{40}Mg_{17}$ + Beta	706, 719[c]	724	E	L	62.8	0. 2	37.0
L ↔ Gamma + $La_3Al_{40}Mg_{17}$ + Beta	709	724	E	L	60.1	0. 2	39.7
L + α-$Al_{11}La_3$ + FCC ↔ $Al_{40}La_3Mg_{17}$		739	P	L	65.5	0. 3	34.2
L + La_2Mg_{17} ↔ Laves_C15 + La(Mg,Al)$_{12}$		903	U	L	2.3	8.7	89.0
L ↔ HCP + Gamma + α-$Al_{11}La_3$	705	711	E	L	30	0. 1	69.9
L + α-$Al_{11}La_3$ + $La_3Al_{40}Mg_{17}$ ↔ Gamma		730	P	L	54.6	0. 2	45.2
L + La_2Mg_{17} + La_5Mg_{41} ↔ Laves_C15		920	P	L	2.3	13.1	84.6

[a] P: peritectic, U: quasiperitectic, E: eutectic.
[b] Experimental data were taken from Odinaev *et al.* [24] unless another reference is given.
[c] Experimental data were taken from Hosseinifar and Malakhov [8].

TABLE 5
Model parameters of the Modified Quasichemical Model used for liquid alloys.

Coordination numbers				References
i	J	Z^i_{ij}	Z^j_{ij}	
Al	Al	6	6	[15]
Ce	Ce	6	6	[15]
La	La	6	6	[15]
Pr	Pr	6	6	[15]
Nd	Nd	6	6	[15]
Sm	Sm	6	6	[15]
Mg	Mg	6	6	[16]
Al	Ce	3	6	[15]
Al	La	3	6	[15]
Al	Pr	3	6	[15]
Al	Nd	3	6	[15]
Al	Sm	3	6	[15]
Mg	Ce	2	6	[16]
Mg	La	2	6	[16]
Mg	Pr	2	6	[16]
Mg	Nd	2	6	[16]
Mg	Sm	2	6	[16]

[16] except that Mg and Al substitute each other on the first sub-lattice. Mg is introduced in the second sub-lattice [16] since considerable solubility of Mg in $Mg_3Pr_{(cF16)}$ was reported by Saccone *et al.* [61] using a Smith thermal analysis technique.

For the BCC_B2 phase, as is known, all Mg–RE binary systems, except for the Mg–Yb binary system, contain the BCC_B2 phase (prototype CsCl) while all AlRE phases in the Al–RE binary systems do not have this CsCl structure. The initial guess of Gibbs energy of the metastable AlRE-BCC_B2 phases is based on the assumption that the difference of energy between two different structures (stable AlRE structure and AlRE-BCC_B2 structure) are the same as the one calculated by Gao *et al.* [62] using first-principles and the entropy of formation of metastable AlRE-BCC_B2 phases was assumed to be the same as the one from the corresponding stable phase. Then, the Gibbs energy of the metastable AlRE-BCC_B2 phases is optimized to fit the available ternary experimental data. In the present study, the BCC_B2 phase was modelled using two sub-lattice CEF with (Mg, Al)(Mg, La, Ce, . . ., Sm) formula.

For the Laves_C15 phase, all Al–RE and Mg–RE (RE = La, Ce, Pr, Nd, Sm) binary systems studied contain the Laves_C15 phase ($cF24$, prototype Cu_2Mg). A two sub-lattice CEF with (Al, Mg, La, Ce, Pr, Nd, Sm)$_2$(Al, Mg, La, Ce, Pr, Nd, Sm) formula was employed to model the Laves_C15 phase.

For other solid solutions (Al_3RE, $Al_{11}RE_3$, $Mg_{12}RE$, $Mg_{41}RE_5$, and $Mg_{17}RE_2$), Al and Mg atoms were introduced in the first sub-lattice, while the rare earth elements are assumed to mix ideally on the second sub-lattice in each one of these solid solutions, *e.g.*, (Al, Mg)$_3$(La, Ce, Pr, Nd, Sm) for the $Al_3RE_{(hP8)}$ phase. These phases were described as stoichiometric compounds in their binary systems.

TABLE 6
Optimized model parameters for solid solutions in the studied ternary systems (J·mol^{-1}).

Gibbs energies of end members and parameters, ΔG^o/(J·mol^{-1})	References
Laves_C15 (Cu_2Mg-type): (Al,Mg,La,Ce,Pr,Nd,Sm)$_2$[Al,Mg,La,Ce,Pr,Nd,Sm]	
G(Al:Al) = 3*GHSERAL* + 41,840	Al–Mg [14]
G(Al:Mg) = 2*GHSERAL* + *GHSERMG* + 30,000 + 4*T*	
G(Mg:Al) = 2*GHSERMG* + *GHSERAL* + 104,971 − 16.46*T*	
G(Mg:Mg) = 3*GHSERMG* + 15,000	Mg–RE [16]
G(Ce:Ce) = 3*GHSERCE* + 62,760	
G(Ce:Mg) = 2*GHSERCE* + *GHSERMG* + 41,840	
G(La:La) = 3*GHSERLA* + 62,760	
G(La:Mg) = 2*GHSERLA* + *GHSERMG* + 41,840	
G(Pr:Pr) = 3*GHSERPR* + 62,760	
G(Pr:Mg) = 2*GHSERPR* + *GHSERMG* + 41,840	
G(Nd:Nd) = 3*GHSERND* + 62,760	
G(Nd:Mg) = 2*GHSERND* + *GHSERMG* + 41,840	
G(Sm:Sm) = 3*GHSERSM* + 62,760	
G(Sm:Mg) = 2*GHSERSM* + *GHSERMG* + 41,840	
G(Ce:Al) = 2*GHSERCE* + *b* + 41,840	
G(La:Al) = 2*GHSERLA* + *GHSERAL* + 41,840	
G(Pr:Al) = 2*GHSERPR* + *GHSERAL* + 41,840	
G(Nd:Al) = 2*GHSERND* + *GHSERAL* + 41,840	
G(Sm:Al) = 2*GHSERSM* + *GHSERAL* + 41,840	
L(Al,Mg:La) = 20,920($Y_{Al} - Y_{Mg}$) − 20,083($Y_{Al} - Y_{Mg}$)^2	This work
L(Al,Mg:Ce) = −20,920 + 33,890($Y_{Al} - Y_{Mg}$)	This work
L(Al,Mg:Pr) = −4184 + 27,196($Y_{Al} - Y_{Mg}$)	This work
L(Al,Mg:Nd) = −8368 + 33,054($Y_{Al} - Y_{Mg}$)	This work
L(Al,Mg:Sm) = 29,288	This work
BCC_B2 (CsCl-type): (Al,Mg)[Mg,Ce,La,Pr,Nd,Sm]	
G(Al:La) = *GHSERAL* + *GHSERLA* − 79,000 + 5.70*T*	Al–RE [15]
G(Al:Ce) = *GHSERAL* + *GHSERCE* − 82,217 + 12.91*T*	
G(Al:Pr) = *GHSERAL* + *GHSERPR* − 83,496 + 10.34*T*	
G(Al:Nd) = *GHSERAL* + *GHSERND* − 89,092 + 12.81*T*	
G(Al:Sm) = *GHSERAL* + *GHSERSM* − 91,000 + 16.00*T*	
G(Mg:La) = *GHSERMG* + *GHSERLA* − 28,990 + 5.08*T*	Mg–RE [16]
G(Mg:Ce) = *GHSERMG* + *GHSERCE* − 28,600 + 5.08*T*	
G(Mg:Pr) = *GHSERMG* + *GHSERPR* − 28,800 + 5.08*T*	
G(Mg:Nd) = *GHSERMG* + *GHSERND* − 29,291 + 5.08*T*	
G(Mg:Sm) = *GHSERMG* + *GHSERSM* − 28,600 + 5.08*T*	
L(Al,Mg:La) = −25,104	This work
L(Al,Mg:Ce) = −41,840	This work
L(Al,Mg:Pr) = −24,686	This work
L(Al,Mg:Nd) = −23,430	This work
L(Al,Mg:Sm) = −12,552	This work
(La,Ce,Pr,Nd,Sm)[Al,Mg]$_{12}$	
G(Ce:Mg) = *GHSERCE* + 12*GHSERMG* − 74,057 + 11.6*T*	Mg–RE [16]
G(La:Mg) = *GHSERLA* + 12*GHSERMG* − 77,781 + 4.9*T*	
G(Pr:Mg) = *GHSERPR* + 12*GHSERMG* − 72,802 + 14.9*T*	
G(Nd:Mg) = *GHSERND* + 12*GHSERMG* − 59,200 + 14.9*T*	This work
G(Sm:Mg) = *GHSERSM* + 12*GHSERMG* − 45,800 + 14.9*T*	This work
G(Ce:Al) = *GHSERCE* + 12*b* − 168,000 + 11.6*T*	This work
G(La:Al) = *GHSERLA* + 12*GHSERAL* − 186,000 + 6.64*T*	This work
G(Pr:Al) = *GHSERPR* + 12*GHSERAL* − 171,000 + 14.9*T*	This work
G(Nd:Al) = *GHSERND* + 12*GHSERAL* − 164,000 + 14.9*T*	This work
G(Sm:Al) = *GHSERSM* + 12*GHSERAL* − 151,000 + 14.9*T*	This work
L(Ce:Al,Mg) = −167,360	This work
L(La:Al,Mg) = −41,840	This work
Al_3RE (Ni_3Sn) : (Al,Mg)$_3$[La,Ce,Pr,Nd,Sm]	
G(Mg:La) = 3*GHSERMG* + *GHSERLA* − 36,400 + 5.51*T*	This work
G(Mg:Ce) = 3*GHSERMG* + *GHSERCE* − 40,800 + 12.6*T*	This work
G(Mg:Pr) = 3*GHSERMG* + *GHSERPR* − 39,600 + 19.1*T*	This work
G(Mg:Nd) = 3*GHSERMG* + *GHSERND* − 38,400 + 20.6*T*	This work
G(Mg:Sm) = 3*GHSERMG* + *GHSERSM* − 34,000 + 20.6*T*	This work
L(Al,Mg:La) = 16,736	This work
L(Al,Mg:Ce) = 16,736	This work
$Al_{11}RE_3$ ($\alpha Al_{11}La_3$) : (Al,Mg)$_{11}$[La,Ce,Pr,Nd,Sm]$_3$	
G(Al:La) = 11*GHSERAL* + 3*GHSERLA* − 575,000 + 8.6*T*	
G(Al:Ce) = 11*GHSERAL* + 3*GHSERCE* − 610,000 + 39.0*T*	
G(Al:Pr) = 11*GHSERAL* + 3*GHSERPR* − 615,000 + 59.1*T*	Al–RE [15]
G(Al:Nd) = 11*GHSERAL* + 3*GHSERND* − 575,000 + 53.5*T*	
G(Al:Sm) = 11*GHSERAL* + 3*GHSERSM* − 527,000 + 53.5*T*	
G(Mg:La) = 11*GHSERMG* + 3*GHSERLA* − 84,626 + 8.6*T*	This work
G(Mg:Ce) = 11*GHSERMG* + 3*GHSERCE* − 69,550 + 39.0*T*	This work
G(Mg:Pr) = 11*GHSERMG* + 3*GHSERPR* − 58,800 + 53.5*T*	This work
G(Mg:Nd) = 11*GHSERMG* + 3*GHSERND* − 48,700 + 53.5*T*	This work
G(Mg:Sm) = 11*GHSERMG* + 3*GHSERSM* − 38,885 + 53.5*T*	This work

TABLE 6 (*continued*)

Gibbs energies of end members and parameters, ΔG^o/(J·mol^{-1})	References
$Al_{17}RE_2$ ($Ni_{17}Th_2$) : (Al,Mg)$_{17}$[La,Ce,Pr,Nd,Sm]$_2$	
G(Al:La) = 17*GHSERAL* + 2*GHSERLA* − 298,692 + 5.7*T*	
G(Al:Ce) = 17*GHSERAL* + 2*GHSERCE* − 292,732 + 26.0*T*	
G(Al:Pr) = 17*GHSERAL* + 2*GHSERPR* − 289,945 + 39.4*T*	This work
G(Al:Nd) = 17*GHSERAL* + 2*GHSERND* − 322,546 + 35.7*T*	
G(Al:Sm) = 17*GHSERAL* + 2*GHSERSM* − 287,564 + 59.8*T*	

In the Al–Mg system [14], there are liquid, FCC, HCP, Gamma ($Al_{12}Mg_{17}$), Beta ($Al_{140}Mg_{89}$), and Epsilon ($Al_{30}Mg_{23}$) phases.

3.4. Estimations on Gibbs free energy of metastable end-members in solid solutions

The difference of enthalpy of formation at T = 298 K between the metastable phases Mg_3La, Mg_3Ce, Mg_3Pr, Mg_3Nd and Mg_3Sm in the Ni_3Sn-hP8 structure and the stable phases (Mg_3La, Mg_3Ce, Mg_3Pr, Mg_3Nd and Mg_3Sm in the BiF_3-cF16 structure) was taken from the results of *ab initio* calculations by Tao [63,64], while the entropy of formation at T = 298 K for these metastable phases are assumed to be the same as the ones calculated from their respective stable phases. As to the enthalpy of formation at T = 0 K for $Mg_3La_{(cF16)}$ phase, it was noted that *ab initio* calculations by Tao [63,64] (−13.1 kJ·gatom^{-1}) and by Taylor *et al.* [65,66] (−13.5 kJ·gatom^{-1}) gave very similar results. The $Mg_{11}RE_3$ phase in the $\alpha Al_{11}La_3$-oI28 structure, the $Al_{12}RE$ phase in the $Mg_{12}Ce$-oI338 structure, the $Al_{17}RE_2$inthe $Ni_{17}Th_2$-hP38 structure, and the $Al_{41}RE_5$phase (RE = La, Ce, Pr, Nd, Sm) in the $Mg_{41}Ce_5$-tI92 structure are calculated using the Miedema model and the results are shown in table 2.The entropy of formation at T = 298 K of the $Mg_{11}RE_3$ phases in the $\alpha Al_{11}La_3$-oI28 structure is linearly interpolated between the entropy of the stable Mg_3RE and $Mg_{41}RE_5$(RE = La, Ce, Pr, Nd) phases or between the entropy of the stable Mg_3Sm and Al_5Sm compound at T = 298 K. The entropy of formation at 298 K of the $Al_{12}RE$ phases in the $Mg_{12}Ce$-oI338 structure, the $Al_{17}RE_2$ phases in the $Ni_{17}Th_2$-hP38 structure, and the $Al_{41}RE_5$ phases (RE = La, Ce, Pr, Nd, Sm) in the $Mg_{41}Ce_5$-tI92 structure is linearly interpolated between the entropy of Al and the entropy of the Al-richest stable compound (that is $Al_{11}RE_3$ where RE is La, Ce, Pr and Nd, Al_3Sm) at 298 K.

4. Results and discussions

4.1. Experimental results

The experimental results of microanalysis on ten key alloys (A1, A2... A10) are listed in table 3.Backscattered electron images of two key alloys (A1, A2) in the Al–Mg–La system annealed at T = 673 K for four weeks are shown in figures 1 and 2. The compositions of the phases detected have been measured by EPMA (table 3). The stability of the $Mg_{12}La$ phase at 673 Kwas confirmed and the solid solubility of Al in this phase is found to be small. Shown in figure 2 is a microphotograph of sample A2, where three phases ((Al), $Al_{11}La_3$, ternary phase (noted as τ1)) are in equilibrium at 673 K. The composition of the ternary τ1 phase in the A2 sample is close to the stoichiometry $Al_{40}Mg_{17}La_3$, which is used in the present optimization. This ternary phase corresponds to the $Al_2Mg_{0.85}La_{0.15}$ proposed by Odinaev *et al.* [23].

A backscattered electron image of the solid-solid Al_2Ce–MgCe diffusion couple annealed at T = 673 K for 10 weeks is shown in figure 3. Unfortunately, some phases (probably Mg_3Ce and $Mg_{41}Ce_5$ intermetallic compounds) in the solid-solid Al_2Ce–MgCe diffusion couple were chipped out during the quenching process probably

TABLE 7
Optimized model parameters for stoichiometric compounds.

Compound	$\Delta H°_{298}$/(J·mol^{-1}))	$S°_{298}$ /(J·K^{-1}·mol^{-1})	C_p/(J·K^{-1}·mol^{-1})
$Al_{13}CeMg_6$	−248,368.0	627.48	$C_p = 13C_p(Al,FCC\_A1) + C_p(Ce,FCC\_A1) + 6C_p(Mg,HCP\_A3)$
$Al_{40}Mg_{17}La_3$	−701,000.0	1878.07	$C_p = 40C_p(Al,FCC\_A1) + 17C_p(Mg,HCP\_A3) + 3C_p(La,DHCP)$
$Al_{50}Mg_{22}Pr_3$	−776,101.6	2325.97	$C_p = 50C_p(Al,FCC\_A1) + 22C_p(Mg,HCP\_A3) + 3C_p(Pr,DHCP)$
$Al_{50}Mg_{22}Nd_3$	−738,772.0	2322.99	$C_p = 50C_p(Al,FCC\_A1) + 22C_p(Mg,HCP\_A3) + 3C_p(Nd,DHCP)$

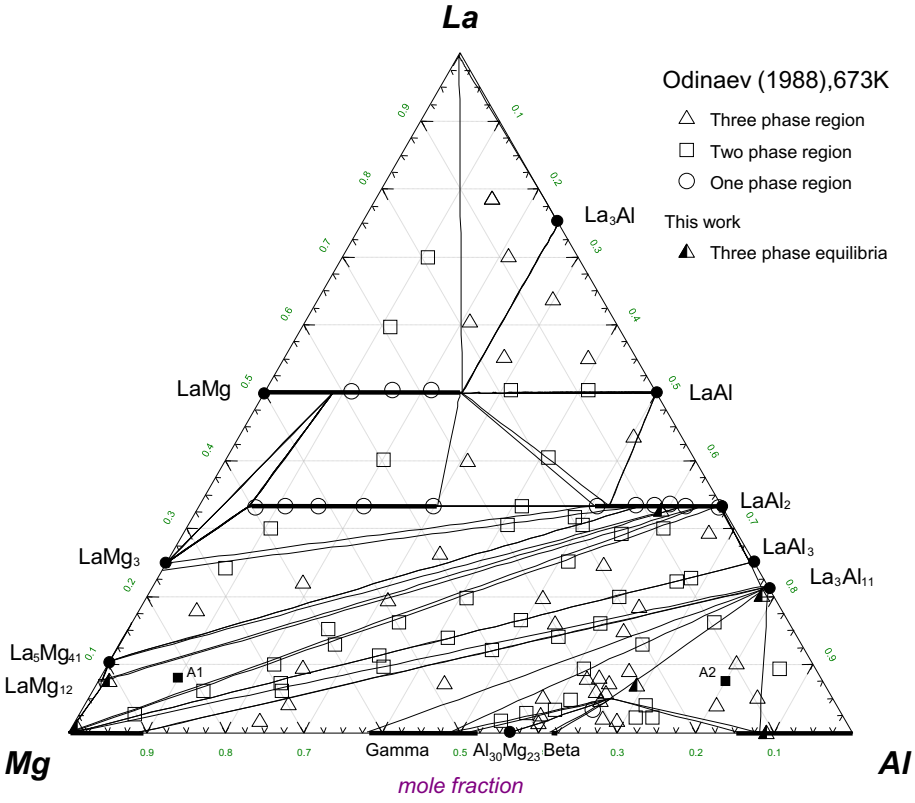

FIGURE 15. The calculated isothermal section of the Mg–Al–La ternary system at $T = 673$ K compared with experimental data of Odinaev *et al.* [23].

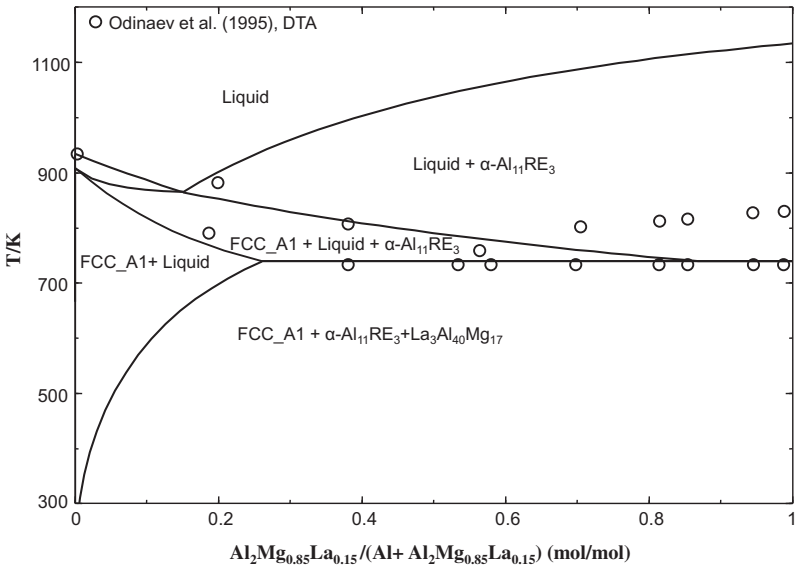

FIGURE 16. Calculated Al–$Al_2Mg_{0.85}La_{0.15}$ section compared with experimental data of Odinaev *et al.* [24].

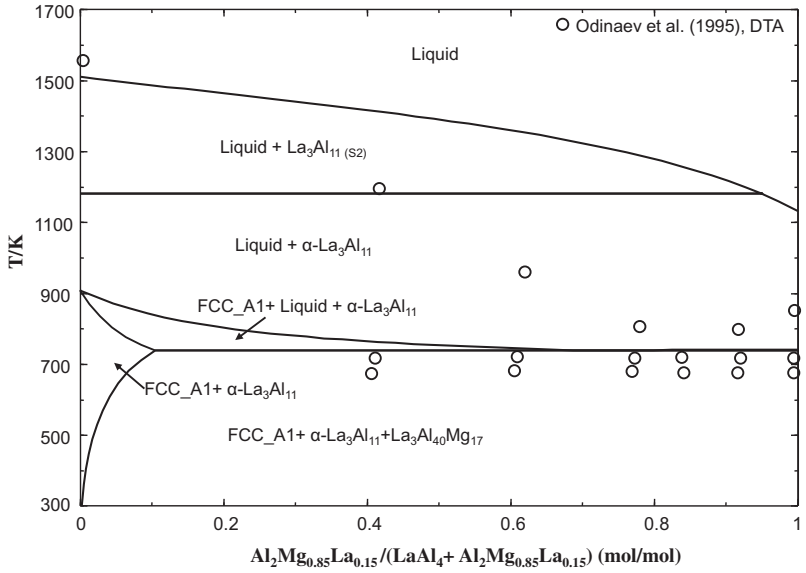

FIGURE 17. Calculated $LaAl_4$–$Al_2Mg_{0.85}La_{0.15}$ section compared with experimental data of Odinaev *et al.* [24] ($LaAl_4$ represents a composition, not a phase).

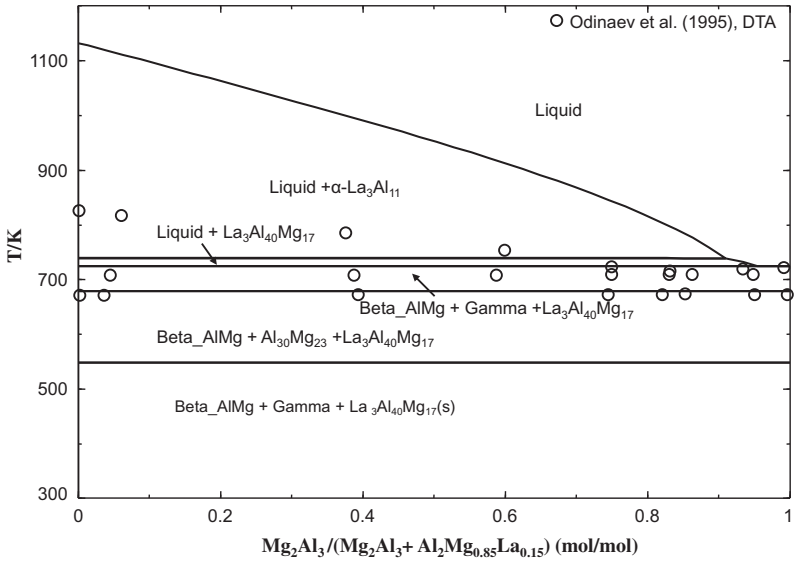

FIGURE 18. Calculated Mg_2Al_3–$Al_2Mg_{0.85}La_{0.15}$ section compared with experimental data of Odinaev *et al.* [24].

due to their brittleness. The composition profiles from the result of EPMA 26 μm line scan of the diffusion couple are shown in figure 4. Three phases were identified: BCC_B2, Laves_C15 and the Al_2Ce compound. One tie-line between BCC_B2 and Laves_C15 is established. Backscattered electron images of two key alloys (A3, A4) in the Al–Mg–Ce system annealed at 673 K for four weeks were shown in figures 5(a), (b) and 6, respectively. The identified phases and microanalysis data are listed in table 3. Three phases (Al-FCC solid solution, a ternary phase (noted as τ2) and the $Al_{11}Ce_3$ compound) are in equilibrium at 673 K as shown in figure 5. The composition of the ternary phase (τ2) is close to $Al_{13}Mg_6Ce$ proposed by Gröbner *et al.* [9], which corresponds to the $Al_2Mg_{0.8}Ce_{0.2}$ reported by Odinaev *et al.* [28]. One tie-line was constructed between BCC_B2 and Laves_C15 from figure 6, which is also consistent with the results of Gröbner *et al.* [9].

For the Al–Mg–Pr system, four key alloys (A5, A6, A7, and A8) annealed at $T = 673$ K for four weeks were investigated. Only the backscattered electron images for key alloys A5 and A8 are shown in figures 7 and 8 respectively. Their microanalysis data are listed in table 3. The solid solubility of Al in $Mg_{12}Pr$ phase is negligible, unlike in $Mg_{12}La$ and $Mg_{12}Ce$. This is consistent with the phase equilibria determined by Odinaev *et al.* [34]. A small amount of Mg in the $(Mg,Al)_3Pr$ solid solution is detected and used in the present optimization. This characteristic is similar to the $(Mg,Al)_3$-La phase. The microstructure of sample A8, which is in a three-phase field, is shown in figure 8, where the presence of a ternary phase (τ3) in the Al-rich region is highlighted. The average composition of this ternary phase is close to the stoichiometry $Al_2Mg_{0.88}Pr_{0.12}$ [33], which is labelled as $Al_{50}Mg_{22}Pr_3$ in the present study.

For the Al–Mg–Nd system, two key alloys (A9,A10) annealed at $T = 673$ K for four weeks are studied. Only the backscattered electron image for alloy A9 is shown in figure 9. The solid solubility of Nd in the Gamma phase is negligible. A small solubility of Mg in $(Mg,Al)_{11}Nd_3$ is observed (see table 3). Negligible solid solubility of Al in $Mg_{41}Nd_5$ phase is detected.

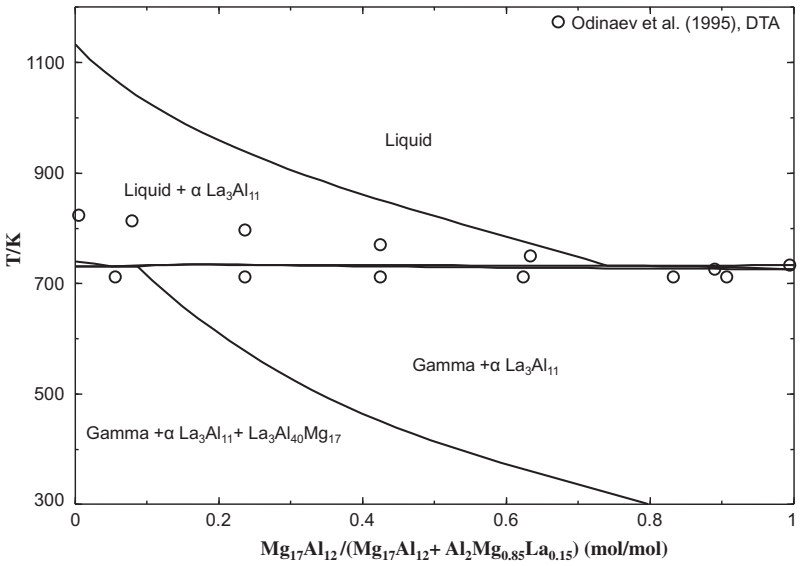

FIGURE 19. Calculated $Mg_{17}Al_{12}$–$Al_2Mg_{0.85}La_{0.15}$ section compared with experimental data of Odinaev *et al.* [24].

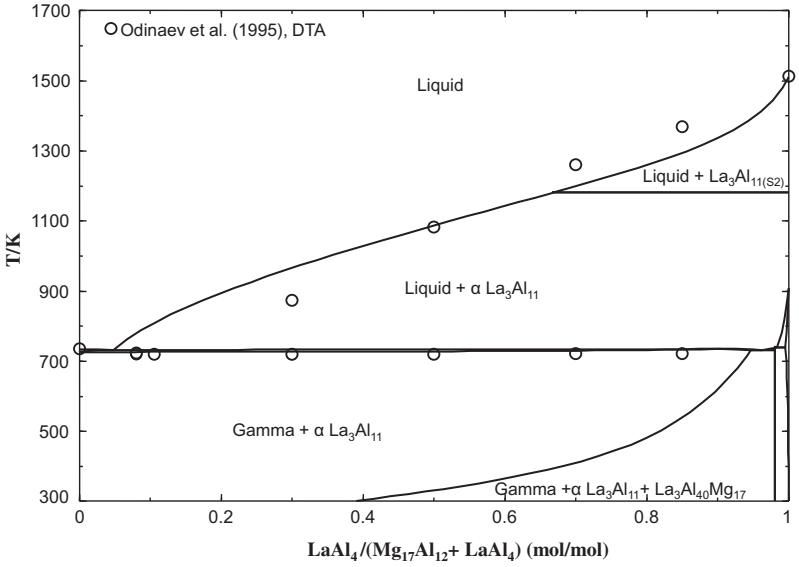

FIGURE 20. Calculated $LaAl_4$-$Mg_{17}Al_{12}$ section compared with experimental data of Odinaev *et al.* [24] ($LaAl_4$ represents a composition, not a phase).

It was worth noting that the ternary phases $Al_{40}Mg_{17}La_3$ (τ1), $Al_{13}Mg_6Ce$ (τ2), and $Al_{50}Mg_{22}Pr_3$ (τ3) are formed in quasi-peritectic reactions and that these reactions are almost complete as can be seen from the phase compositions in table 3.

All the phases observed and their compositions are considered in the present optimization.

4.2. Thermodynamic optimizations of Al–Mg–RE (La, Ce, Pr, Nd, Sm) ternary systems

Table 2 shows the estimated enthalpies of formation of the stable ternary compounds ($Al_{40}Mg_{17}La_3$, $Al_{13}Mg_6Ce$, $Al_{50}Mg_{22}Pr_3$ and $Al_{50}Mg_{22}Nd_3$) from the Miedema model, which are used as initial guesses for the thermodynamic optimizations. The entropies of formation of these four ternary compounds are estimated from the contribution of $Al_{11}RE_3$ and Mg_xAl_y alloy (x, y is calculated by mass balance) in Mg–Al–$Al_{11}RE_3$ system. The enthalpies of formation of these ternary phases were then optimized in order to obtain satisfactory results for phase equilibria. As is seen in table 2, the hypothetical phases ($Al_{12}La$, $Al_{12}Ce$, $Al_{12}Pr$, $Al_{12}Nd$ and $Al_{12}Sm$) in the $Mg_{12}Ce$-oI338 structure, which are the end-members of the $(Mg, Al)_{12}(La, Ce, Pr, Nd,Sm)$ solid solution ($Mg_{12}Ce$-oI338) are also estimated from the Miedema model together with other hypothetical phases like $Mg_{11}RE_3$ phase in the $\alpha Al_{11}La_3$-oI28 structure, and $Al_{41}RE_5$ phase in the *tI*92-$Mg_{41}Ce_5$ structure.

Due to great importance of the HCP_A3solid solution in Mg alloys, the enthalpy of mixing of the HCP_A3solution in the Al–RE (RE = La, Ce, Pr, Nd, Sm) subsystems are also estimated using the Miedema model. The Gibbs energy of the HCP_A3solution, which is supposed to be less stable than the DHCP solution in the Al–RE systems, has to be evaluated although it is not stable in the Al–RE (RE = La, Ce, Pr, Nd, Sm) phase diagrams. Figures 10–14 show the optimized enthalpies of mixing of HCP_A3 solution in the Al–RE (RE = La, Ce, Pr, Nd, Sm) respectively, compared with the enthal-

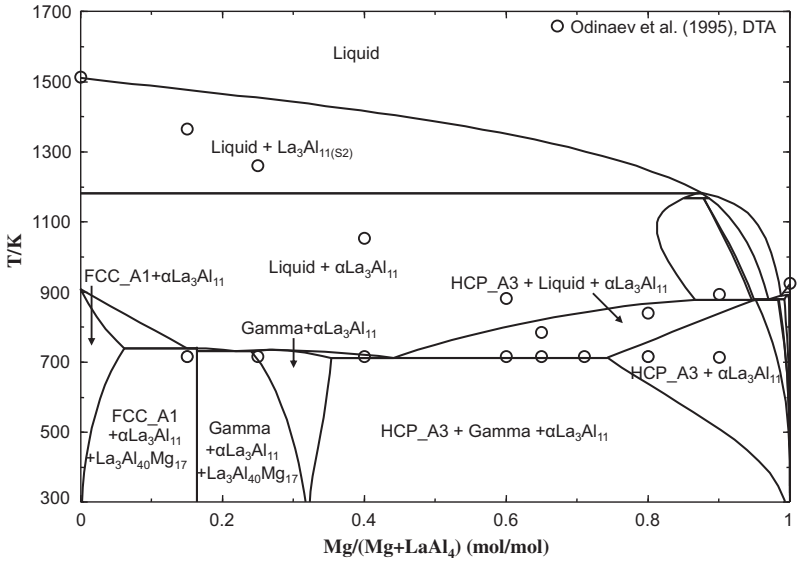

FIGURE 21. Calculated $LaAl_4$–Mg section compared with experimental data of Odinaev *et al.* [24] ($LaAl_4$ represents a composition, not a phase).

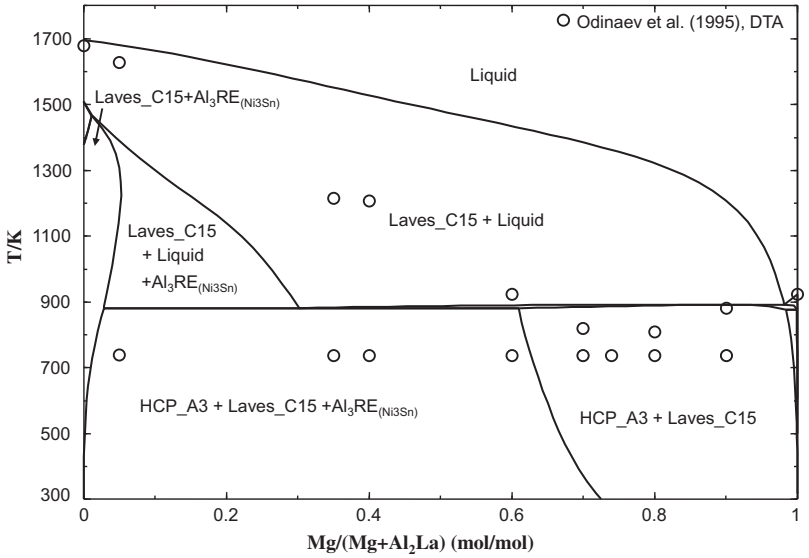

FIGURE 22. Calculated $LaAl_2$–Mg section compared with experimental data of Odinaev *et al.* [24].

pies of mixing of the liquid at $T = 1500$ K in the Al–RE systems and the estimated enthalpies of mixing from the Miedema model.

Since new optimizations of the Al–RE (RE = La, Ce, Pr, Nd, Sm) [15] and Mg–RE [16] binary systems are carried out using the Modified Quasichemical Model for the liquid phase, the thermodynamic properties and phase diagram of the Mg–Al–RE system are calculated by combining our two new optimizations with the previous optimization for the Al–Mg system by Chartrand [14]. In the Al–Mg system by Chartrand [14], there are liquid, FCC, HCP, Gamma ($Al_{12}Mg_{17}$), Beta ($Al_{140}Mg_{89}$), and Epsilon ($Al_{30}Mg_{23}$) phases. As shown in table 1, two sub-lattices were used for all the solid solution phases involved in the present study.

Laves_C15 and BCC_B2 phases appears in all the Mg–Al–RE (RE = La, Ce, Pr, Nd, Sm) isothermal sections at $T = 673$ K. For the Laves_C15 phase, two optimized interaction parameters for the Al and Mg mixing in the first sub-lattice were required in order to reproduce the observed miscibility gap by Odinaev *et al.* [23] at 673 K. The Laves phases observed in the binary systems Al_2RE and Mg_2RE are expected to show negligible deviations from stoichiometry. In other words, the phases can be described as stoichiometric compounds in the binary systems. Therefore, $G^0_{Al_2RE}$ and $G^0_{Mg_2RE}$ were set equal to the Gibbs energy of the corresponding stoichiometric compounds Al_2RE and Mg_2RE; the Gibbs energies of other end members were taken either from the COST–507 database [67], or were set to arbitrarily large values as shown in table 6. For the BCC_B2 phase, G^0_{AlRE} was used as a model parameter to reproduce the Al solubility measured by Odinaev *et al.* [23]; other Gibbs energies were either taken from the binary optimization in the RE–Mg system [16] or were set to arbitrarily large values. One interaction parameter was necessary to reproduce the 2-phase equilibria between the BCC_B2 and pure RE phases at 673 K (table 6).

It is worth noting that liquidus experimental data are available only for the Al–Mg–Al_2RE systems. In the present study, thermodynamic properties in the region of $X_{RE} > 1/3$ are estimated. Only invariant reactions of the Al–Mg–RE system for $X_{RE} < 1/3$ are listed.

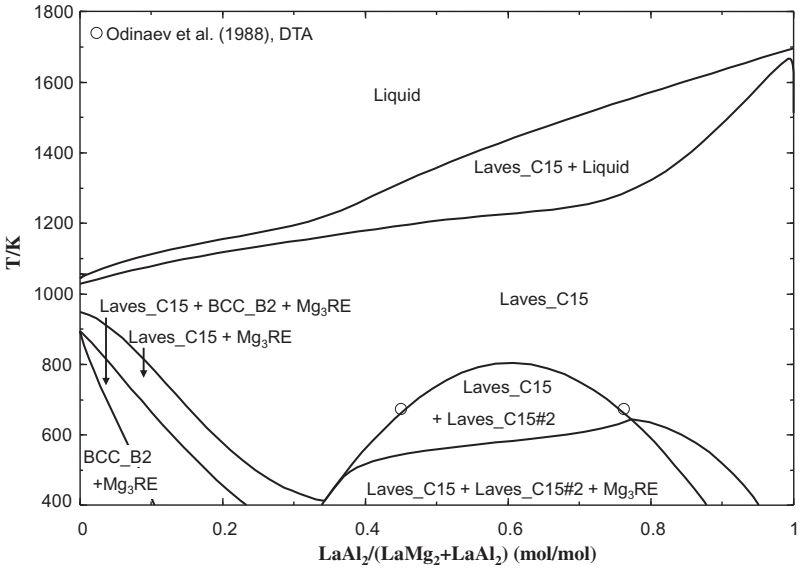

FIGURE 23. Calculated $LaAl_2$–$LaMg_2$ section compared with experimental data of Odinaev *et al.* [24].

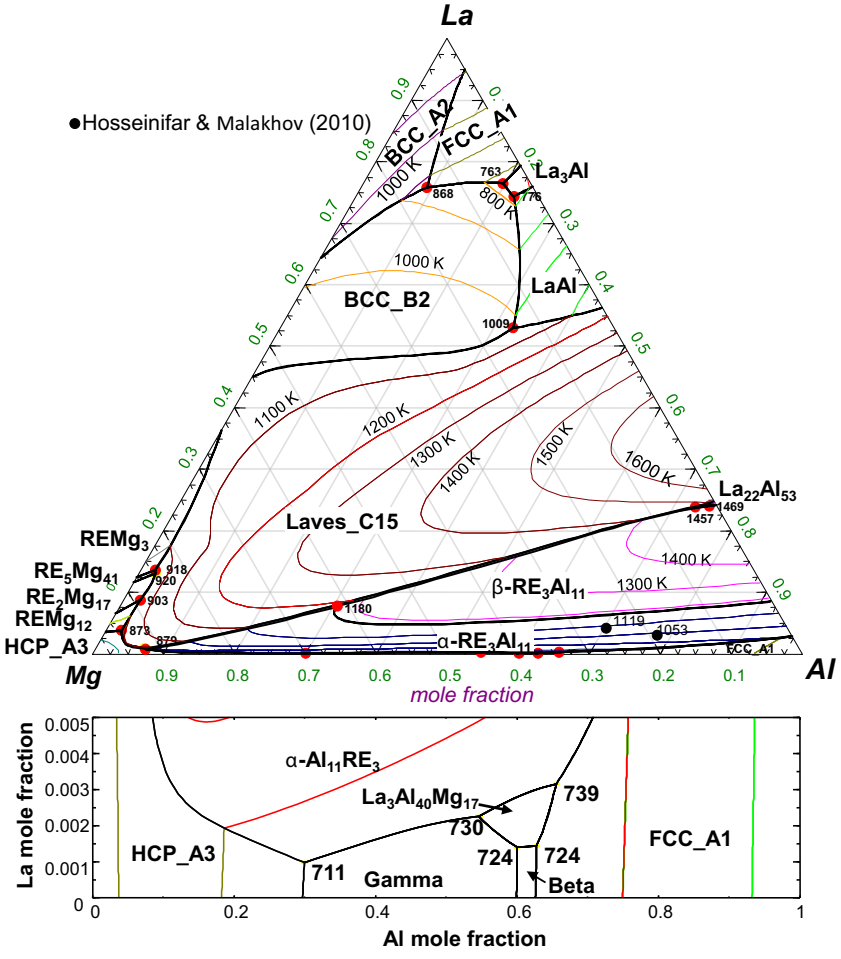

FIGURE 24. The liquidus projection of the Al–Mg–La system with experimental data of Hosseinifar and Malakhov [8].

4.2.1. The Al–Mg–La system

The Al–Mg–La ternary system has been reviewed by Raghavan [21]. Recently, Hosseinifar and Malakhov [8] thermodynamically optimized this system to conduct a feasibility study to produce a new material containing a ductile FCC matrix with LaMg (BCC_B2) intermetallic via casting. In their study, they partially revised the Mg–La system and optimized the Al–Mg–La ternary system based on the optimized Al–Mg system from Liang *et al.* [68], the optimized Mg–La system from Guo and Du [25] using the substitutional solution model with Redlich–Kister formalism to describe

TABLE 8
Some invariant reactions of the Al–Mg–Ce system for $X_{Ce} < 1/3$.

Reaction	T/K		Type[a]	Composition/(at.%)			
	Exp.[b]	Calc.		Phase	Calc.		
					Al	Ce	Mg
L + Laves_C15 ↔ HCP + Al_3Ce		892	U	L	4.6	1.0	94.4
L + Al_3Ce ↔ α-$Al_{11}Ce_3$ + HCP		890	U	L	5.2	0.8	94.0
L + HCP ↔ Laves_C15 + $Ce(Mg,Al)_{12}$		875	U	L	2.1	3.3	94.6
L + FCC ↔ $Al_{13}CeMg_6$ + Beta	714 719 [27][c]	723	U	L	63.0	0.3	36.7
L ↔ Gamma + $Al_{11}CeMg_6$ + Beta	715	723	E	L	60.1	0.3	39.6
L + α-$Al_{11}Ce_3$ ↔ FCC + $Al_{13}CeMg_6$	718 728 [7]	734	U	L	65.4	0.6	34.0
L + Ce_5Mg_{41} ↔ Laves_C15 + $Ce(Mg, Al)_{12}$		881	U	L	0.8	8.6	90.6
L ↔ HCP + Gamma + α-$Al_{11}Ce_3$		711	E	L	30.1	0.1	69.8
L + α-$Al_{11}Ce_3$ + $Al_{13}CeMg_6$ ↔ Gamma		730	P	L	53.9	0.4	45.7
L + $CeMg_3$ ↔ Laves_C15 + Ce_5Mg_{41}		893	U	L	4.6	1.0	94.4

[a] P: peritectic, U: quasiperitectic, E: eutectic.
[b] Experimental data were taken from Odinaev *et al.* [31] unless another reference is given.
[c] Reported reaction is L ↔ (Al) + Al_4Ce + Al_8Mg_5 from Zheng *et al.* [32].

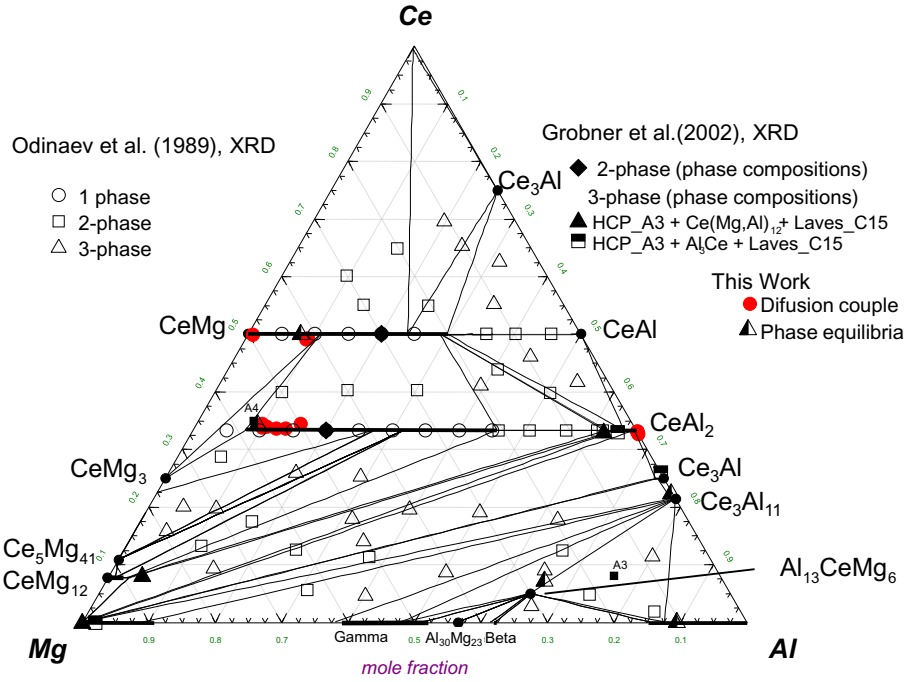

FIGURE 25. The calculated isothermal section of the Mg–Al–Ce ternary system at T = 673 K compared with experimental data of Odinaev *et al.* [28] and Gröbner *et al.* [9].

the excess Gibbs energy for Al–Mg and Mg–La liquid solutions, and the optimized Al–La system from Zhou and Napolitano [69] using an associate model for the liquid with Al, La and Al_2La as mixing species. They used Muggianu method [45] for the evaluation of the Al–Mg–Laternary liquid [8]. In the present study, the Al–Mg–La system was optimized based on our previous optimizations for the Al–La [15], Al–Mg [14], Mg–La [16] binary systems. The Modified Quasi-chemical Model was used for all the liquid where short-range ordering is taken into account. It is believed to be more realistic than the associate model.

It is worth noting that $LaMg_{12}$ was treated as a stoichiometric compound in the Mg–La system [16]. Giovannini *et al.* [70] re-investigated the Mg-rich region of the Mg–La system and found the intermetallic compound $LaMg_{12}$ with oI338-$CeMg_{12}$ structure. Darriet *et al.* [26] and Denys *et al.* [71] obtained a broad homogeneity range for the $LaMg_{12}$ phase. It was reported by Poletaev *et al.* [72] that the $LaMg_{12-x}$alloy crystallized with three different structure modifications depending on the cooling rate: hexagonal $TbCu_7$ with highest cooling rate, tetragonal $ThMn_{12}$ with medium cooling rate, and orthorhombic $LaMg_{11}$ with lowest cooling rate.

The ternary compound, $Al_{40}Mg_{17}La_3$ (noted as $Al_2Mg_{0.85}La_{0.15}$ in [23]), was assumed to be a stoichiometric compound.

The invariant reactions for $X_{La} < 1/3$ are listed in table 4 and compared with the available experimental data [24]. The Gibbs energy of the liquid phase was calculated using the symmetric Kohler-like approximation with no ternary interaction parameters. The optimized model parameters are summarized in tables 5–7.

For the $Mg_{12}RE$ solid solution, $G^{\circ}_{Al_{12}La}$ and a binary parameter (table 6) for the mixing of Al and Mg in one sub-lattice is used to fit the experimental data on the solid solubility of Al. For all solution phases, no ternary parameters were required. The Gibbs energy of the $Al_{40}Mg_{17}La_3$ compound, formed with a peritectic reaction as

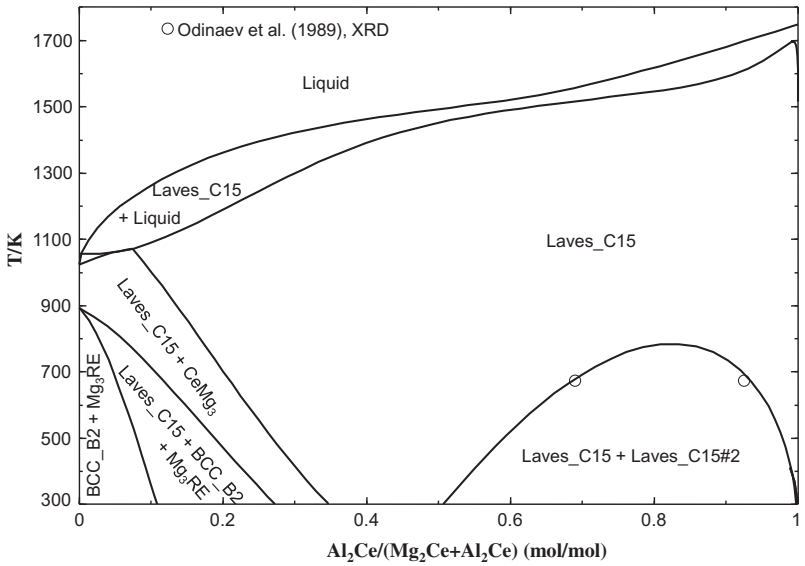

FIGURE 26. Calculated Al_2Ce–Mg_2Ce section compared with experimental data of Odinaev *et al.* [28].

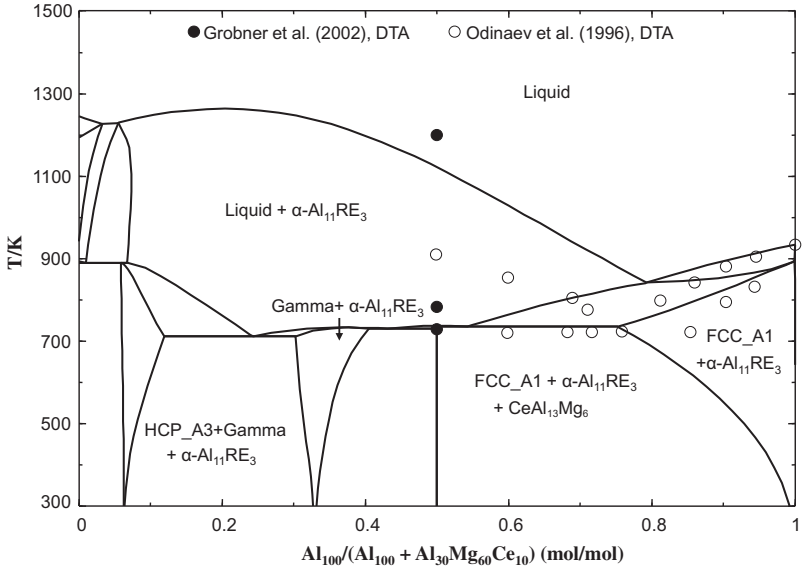

FIGURE 27. Calculated Al_{100}–$Al_{30}Mg_{60}Ce_{10}$ section compared with experimental data of Odinaev *et al.* [31] and Gröbner *et al.* [9].

can be seen in figure 2, was optimized to reproduce the measured phase equilibria at $T = 673$ K. In general, the optimization was directed mainly towards reproducing the phase equilibrium data at 673 K measured by Odinaev *et al.* [23].

A calculated isothermal section of the Mg–Al–La ternary system at $T = 673$ K is shown in figure 15 along with the experimental data of Odinaev *et al.* [23]. LaMg and LaAl are only partially miscible because they have different crystal structures (CsCl and AlCe type, respectively). On the other hand, both $LaMg_2$ and $LaAl_2$ have the Cu_2Mg type structure and they form a Laves_C15 solid solution with a miscibility gap at low temperature. The miscibility gap in the Laves_C15 solution measured by Odinaev *et al.* [23] compares favourably with the present thermodynamic calculation. Most experimental data were well reproduced by present calculations and the agreement between the calculated and experimental sections are satisfactory.

However, there are a few discrepancies between the study of Odinaev *et al.* [23] and the current study. Similar differences were also encountered by Hosseinifar and Malakhov [8].The $LaMg_2$ phase is unstable at $T = 673$ K in the present study. According to Odinaev *et al.* [23], $LaMg_2$ is stable at 673 K. This contradicts the result of Vogel and Heumann [73] who reported that $LaMg_2$ decomposes into $LaMg_3$ and LaMg near $T = 887$ K. However, it is stabilized over a wide temperature range as $LaAl_2$ dissolves into it. Kang *et al.* [16] and Guo and Du [25] considered that the $LaMg_2$ phase is unstable at 673 K. Secondly, the $LaMg_{12}$ and $Al_{30}Mg_{23}$ phases were considered in the current investigation, which were overlooked by Odinaev *et al.* [23]. Finally, the Al_2La and AlLa two-phase equilibrium is only reported to exist in the Al-La binary system by Odinaev *et al.* [23]. However, it is probable that Mg dissolves in Al_2La phase, the reason of which is stated above. Then the Al_2La and AlLa two-phase equilibrium could extend into the ternary region. Moreover, the present interpretation of the microstructure of the anneal alloy $Al_{0.5}Mg_{0.06}La_{0.44}$ did not contradict the observed three-phase field in Odinaev *et al.* [23]. There are two differences between the present calculations and the optimized phase diagram of Hosseinifar and Malakhov [8]. Firstly, the solid solubility of Al in $LaMg_{12}$ was considered in the present study which was evidenced

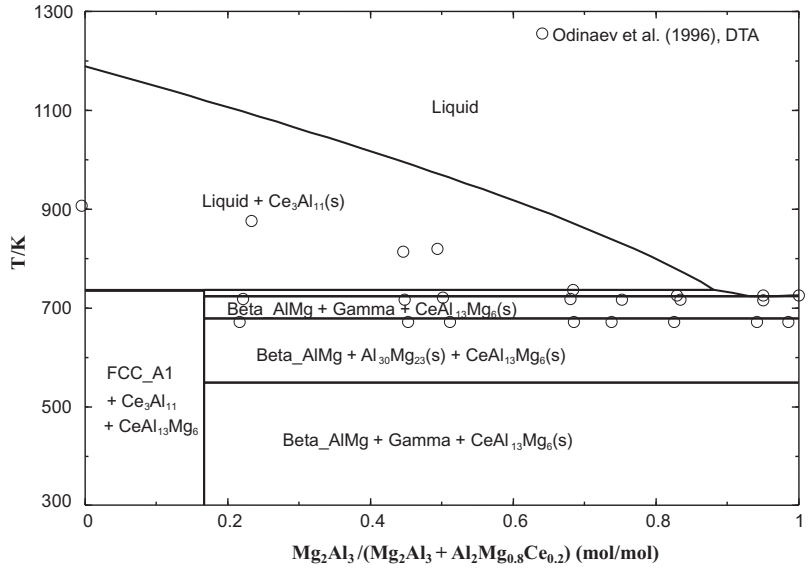

FIGURE 28. Calculated Mg_2Al_3–$Al_2Mg_{0.8}Ce_{0.2}$ section compared with experimental data of Odinaev *et al.* [31].

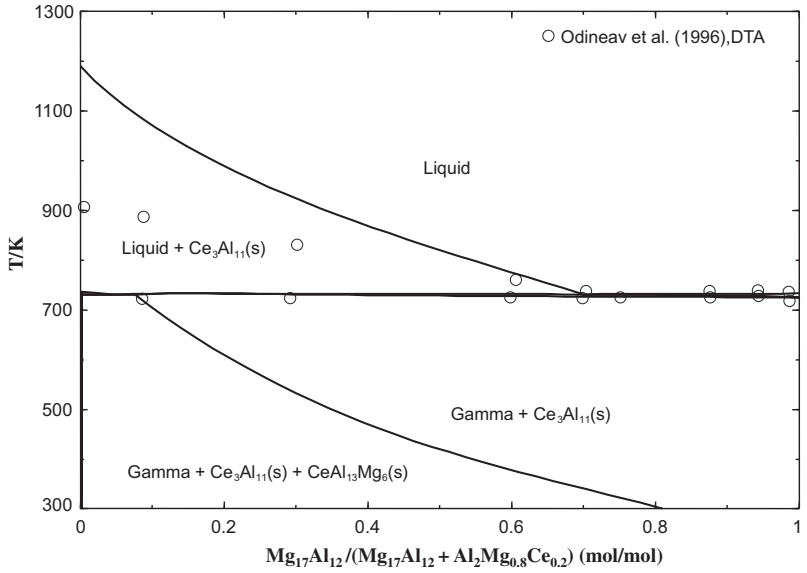

FIGURE 29. Calculated $Mg_{17}Al_{12}$–$Al_2Mg_{0.8}Ce_{0.2}$ section compared with experimental data of Odinaev *et al.* [31].

by the experimental data of Gröbner *et al.* [9]. This modification might be of practical importance to Mg alloys design, since the $LaMg_{12}$ phase could precipitate from the primary Mg phase during the solidification process, the amount of which could affect the mechanical properties of Mg alloy very much. Secondly, the La_5Mg_{41} phase was taken into consideration in the present study.

It is worth noting that a miscibility gap occurred within Laves_C15 phase at $T = 673$ K. This is a common phenomenon for Laves_C15 phases, which was also found in the Al–Mg–Ce, Al–Mg–Pr and Al–Mg–Nd systems.

Figures 16-23 show several calculated sections compared with the experimental DTA data by Odinaev *et al.* [24]. It is observed that the reported liquidus temperatures of Odinaev *et al.* [24] lie far below those from present calculation. Hosseinifar and Malakhov [8] did calorimetric investigation on two alloys ($Al_{61.3}La_{18.7}Mg_{20}$ and $Al_{70.6}La_{14}Mg_{15.4}$ by wt%) to check liquidus temperature in the Al–Mg–La system and their measured values were much higher than those of Odinaev *et al.* [24]. Gröbner *et al.* [9] investigated the liquidus temperature in the Mg–Al–Ce system using DTA and concluded that the low liquidus temperature of Odinaev *et al.* [31] could not be accepted. They pointed out that the reliable DTA data at high temperature can only be obtained by using hermetically sealed inert crucible to avoid evaporation, oxidation and side reactions. Although the experimental details were not given by Odinaev *et al.* [23], their liquidus temperature might be in error due to the oxidation of the rare earth elements, high evaporation of Mg metal, and experimental difficulties at high temperature.

Figure 24 shows the calculated liquidus surface in the Mg–Al–La system with the experimental data from Hosseinifar and Malakhov [8]. It can be seen that the calculated liquidus temperature agrees well with the experimental data [8]. The liquidus surface is dominated by the Laves_C15 (almost pure Al_2La) and $Al_{11}RE_3$phases, which have high melting temperatures and very negative enthal-

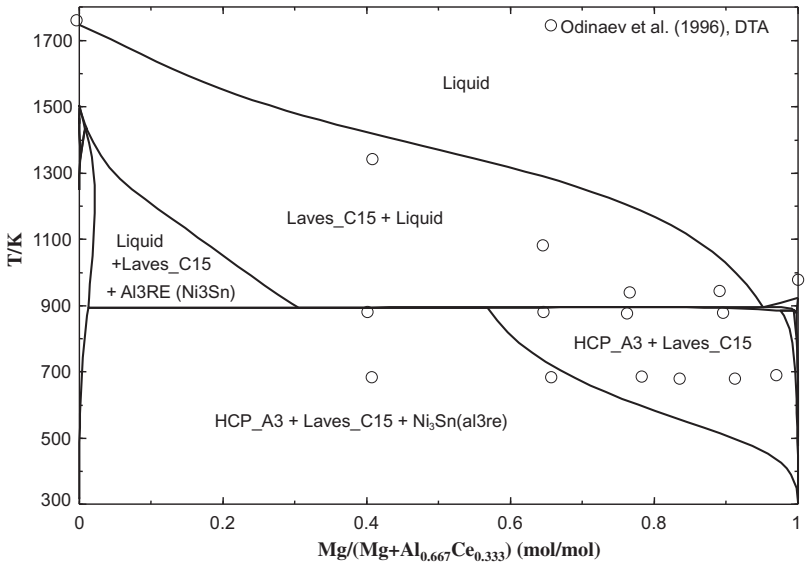

FIGURE 30. Calculated Mg–$Al_{0.667}Ce_{0.333}$ section compared with experimental data of Odinaev *et al.* [31].

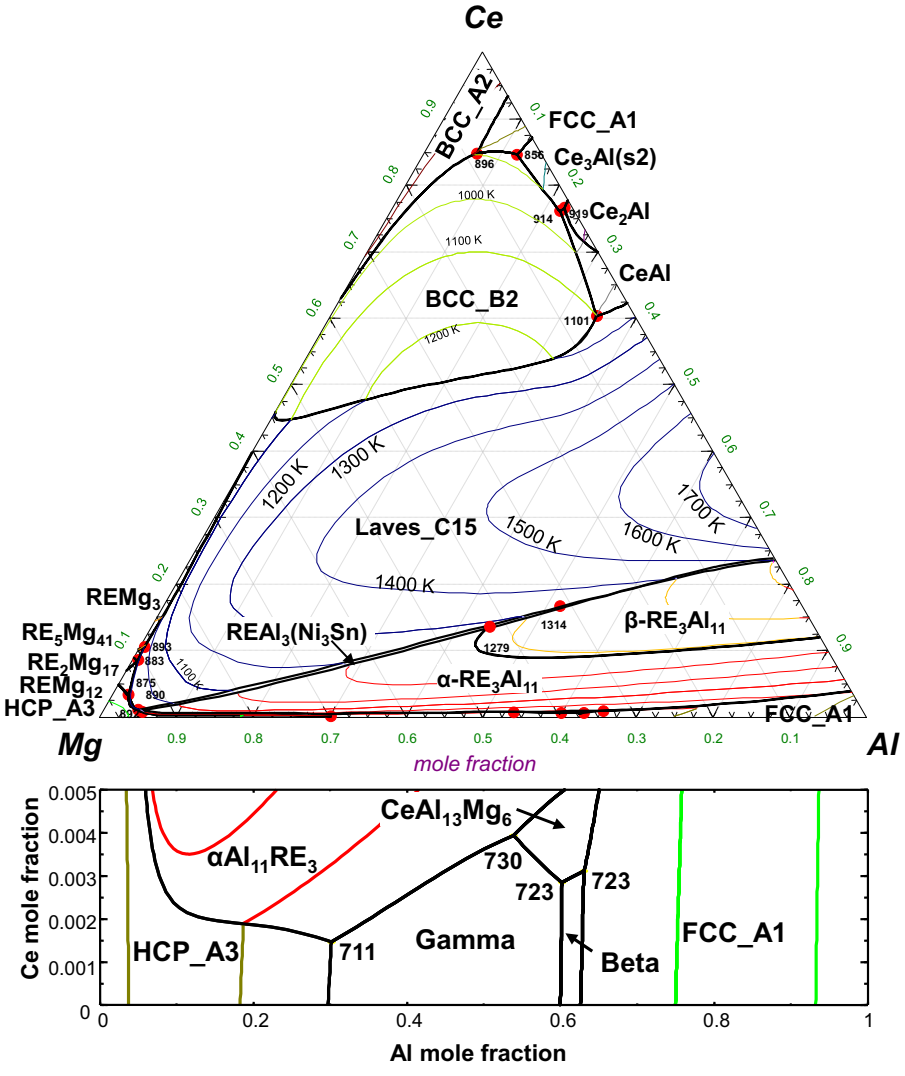

FIGURE 31. The liquidus projection of the Al–Mg–Ce system.

TABLE 9
Some invariant reactions of the Al–Mg–Pr system for $X_{Pr} < 1/3$.

Reaction	T/K		Type[a]	Composition/(at.%)			
	Exp.[b]	Calc.		Phase	Calc.		
					Al	Pr	Mg
L + Pr_5Mg_{41} ↔ Laves_C15 + Mg_3Pr		861	U	L	0.7	10.1	89.2
L ↔ HCP+ Laves_C15 + $Pr(Mg,Al)_{12}$		843	E	L	0.8	6.1	93.1
L + Pr_5Mg_{41} ↔ Laves_C15 + $Pr(Mg,Al)_{12}$		847	U	L	0.8	8.2	91.0
L ↔ Gamma + Beta + $Pr_3Al_{50}Mg_{22}$	709	724	E	L	59.98	0.05	39.97
L + $Al_{11}Pr_3$ + FCC ↔ $Pr_3Al_{50}Mg_{22}$		730	P	L	0.639	0.001	0.36
L ↔ Gamma + HCP_A3 + $Al_{11}Pr_3$	708	712	E	L	29.77	0.03	70.2
L + FCC ↔ Beta + $Pr_3Al_{50}Mg_{22}$		724	U	L	62.64	0.06	37.3
L + $Pr_3Al_{50}Mg_{22}$ + $Al_{11}Pr_3$ ↔ Gamma		726	P	L	58.83	0.07	41.1

[a] P: peritectic, U: quasiperitectic, E: eutectic.
[b] Experimental data were taken from Odinaev *et al.* [35] unless another reference is given.

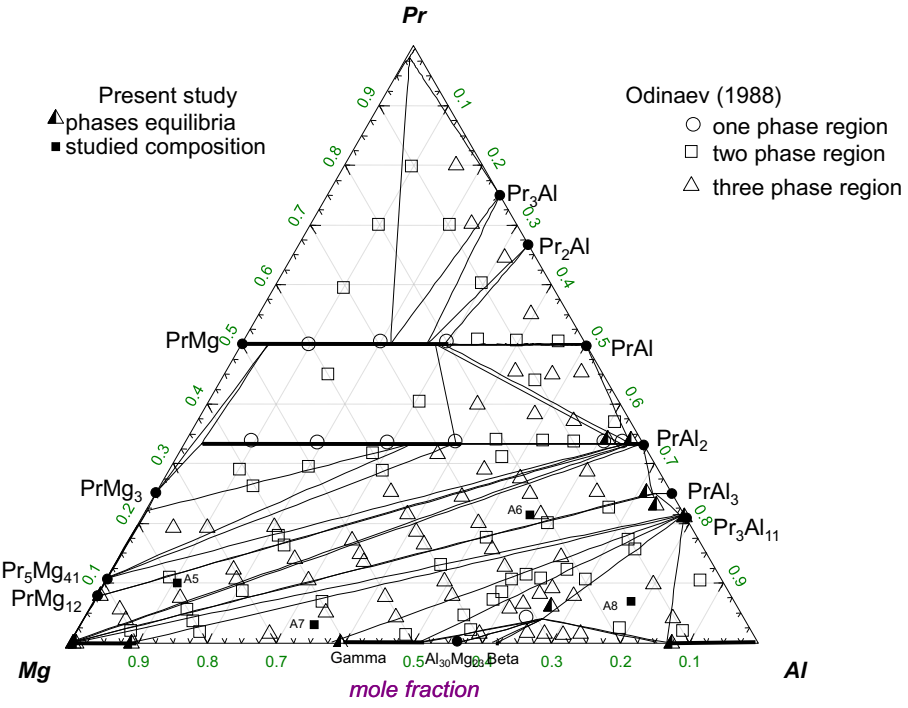

FIGURE 32. The calculated isothermal section of the Mg–Al–Pr ternary system at $T = 673$ K compared with experimental data of Odinaev *et al.* [34].

pies of formations. The primary phase regions of these phases intersect that of Mg(HCP_A3). Therefore, these phases are likely to precipitate in the HCP phase during Mg alloy solidification process. The ternary phase $Al_{40}Mg_{17}La_3$ is formed peritectically (table 4), which is in agreement with our experiment as can be seen in figure 2.

4.2.2. The Al–Mg–Ce system

The Al–Mg–Ce system has been thermodynamically optimized by Gröbner *et al.* [9] without ternary interaction parameters for the liquid phase using a substitutional solution model for the liquid with Muggianu interpolation from three binary sub-systems. Unfortunately, the short-range ordering effect was not considered in the substitutional solution model of their liquid phase. In the present study, MQM is employed for the ternary liquid taking into account the short-range ordering effect and Kohler-type interpolation is used. The ternary compound $Al_{13}CeMg_6$ has a $MgZn_2$ type structure, which is the same as that of the Laves_C14 phase. However, it was assumed to be a stoichiometric (line) compound because no solid solubility has been observed experimentally.

The invariant reactions for $X_{Ce} < 1/3$ are listed in table 8. The Gibbs energy of the liquid phase was calculated using the symmetric Kohler-like approximation [45]with no ternary interaction parameters. The transformation temperature from pure FCC(Ce) to pure DHCP(Ce) was changed by Kang *et al.* [17] from $T = 334$ K (the current value in the COST-507 database [67]) to $T = 283$ K reported in [74]. The optimized model parameters are summarized in tables 5–7.

In order to reproduce the miscibility gap observed for the Laves_C15 phase [28], two optimized interaction parameters were required ($L^0_{Al,Mg:Ce}$, $L^1_{Al,Mg:Ce}$). One interaction parameter was necessary to reproduce the 2-phase equilibria between the BCC_B2 and the FCC_A1 (Ce) phases. For the $Ce(Al,Mg)_{12}$ phase, the Gibbs energy of hypothetical $CeAl_{12}$ and one interaction parameter were optimized in order to reproduce the experimental data. For the other solution phases, no ternary parameters were required. The Gibbs energy of the $Al_{13}CeMg_6$ compound was optimized to reproduce the measured peritectic melting temperature [9]and phase equilibria at $T = 673$ K [28].

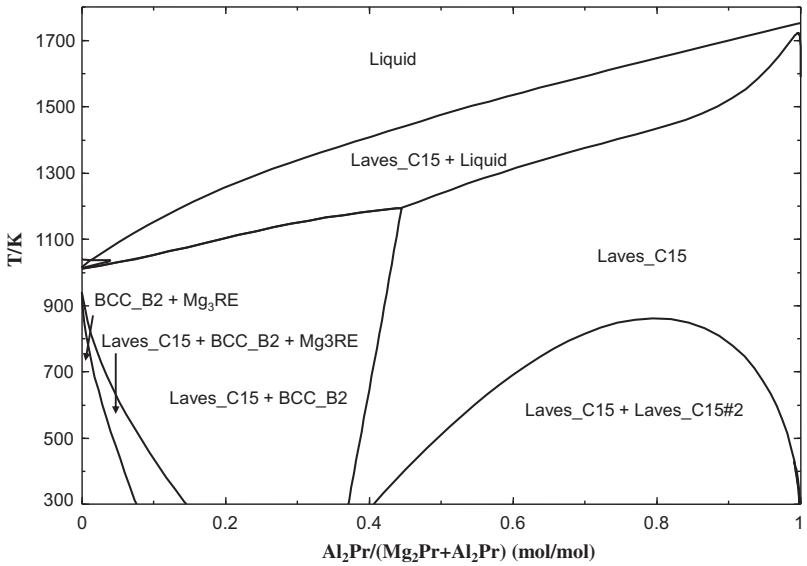

FIGURE 33. The calculated Al_2Pr–Mg_2Pr section.

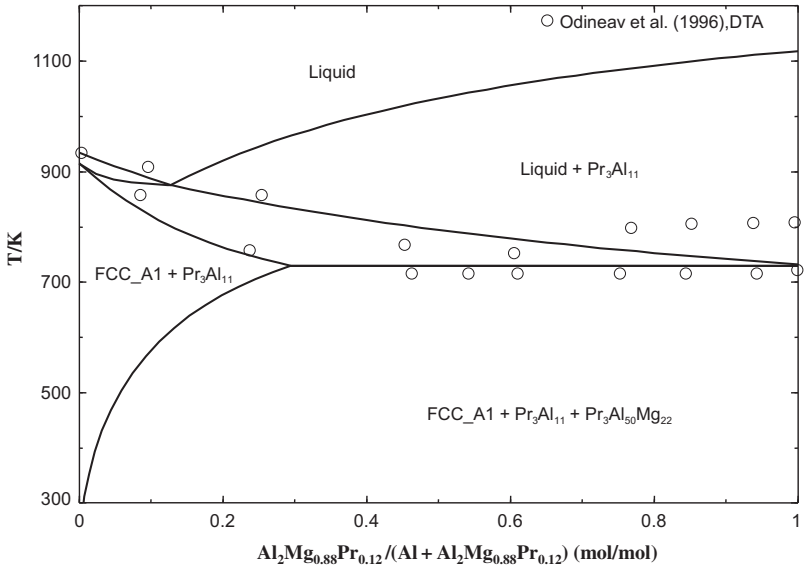

FIGURE 34. Calculated Al–$Al_2Mg_{0.88}Pr_{0.12}$ section compared with experimental data of Odinaev *et al.* [35].

In figure 25, a calculated isothermal section of the Mg–Al–Ce ternary system at $T = 673$ K is shown along with the experimental data of Odinaev *et al.* [28] and Gröbner *et al.* [9]. CeMg and CeAl are only partially miscible since they have different crystal structures (CsCl and AlCe type, respectively). However, $CeMg_2$ and $CeAl_2$ form a Laves_C15 solid solution because they have the same structure (Cu_2Mg type) with a miscibility gap at low temperature. For the isothermal section of the Mg–Al–Ce ternary system at 673 K, most experimental data are well reproduced by current calculations. According to Odinaev *et al.* [28], $CeMg_2$ is stable and forms a solid solution at 673 K. However, this contradicts the result of Vogel and Heumann [73] who reported that $CeMg_2$ decomposes into $CeMg_3$ and CeMg near $T \sim 888$ K. This can be also seen in figure 26, in which the calculated $CeMg_2$–$CeAl_2$ is shown. $CeMg_2$ is only stable over a limited temperature range (891 K ~ 1023 K). However, it is stabilized over a wide temperature range as $CeAl_2$ dissolves into it. The miscibility gap in the Laves_C15 solution measured by Odinaev *et al.* [28] compares favourably with the present thermodynamic calculation.

Figures 27-30 show several calculated sections compared with the experimental DTA data by Odinaev *et al.* [31]and Gröbner *et al.* [9]. In all these figures, it can be observed that the thermodynamic calculations reproduce the temperatures where liquid alloys first form, through either eutectic or peritectic reactions, very closely. However, the reported liquidus temperatures of Odinaev *et al.* [31] are far below the present calculations. Similar discrepancies were also observed in the calculations of the Mg–Al–La and Mg–Al–Y systems, in which experimental DTA data are also available from Odinaev *et al.* [75].

In connection with this, Gröbner *et al.* [9]claimed that the reported liquidus temperatures by Odinaev *et al.* [31]might be in error due to experimental difficulties at high temperature, although the experimental details were not given. Gröbner *et al.* [9] used sealed Ta crucibles in their DTA experiment to measure the liquidus temperature, which we believe is to be more accurate than that of Odinaev *et al.* [31]. As seen in figure 27, the measured liquidus temperatures from two different studies show considerable discrepancy (~290 K). The calculated liquidus temperature in the

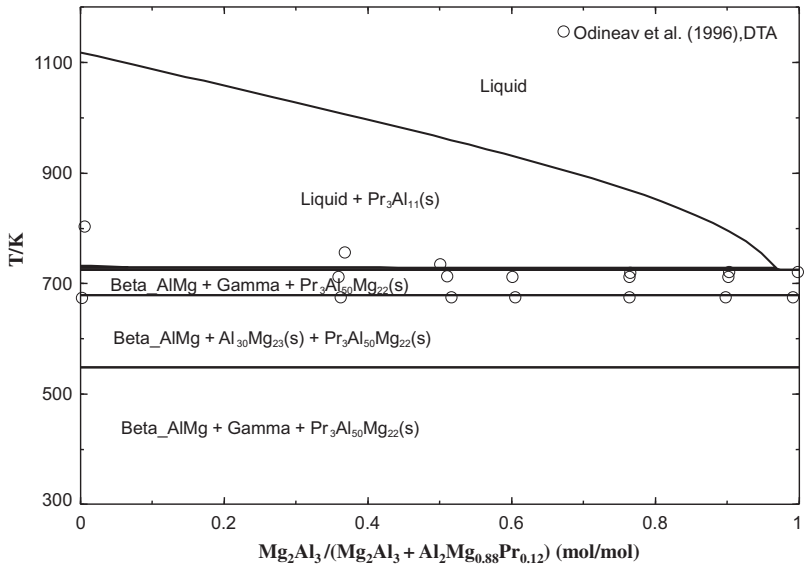

FIGURE 35. Calculated Mg_2Al_3–$Al_2Mg_{0.88}Pr_{0.12}$ section compared with experimental data of Odinaev *et al.* [35].

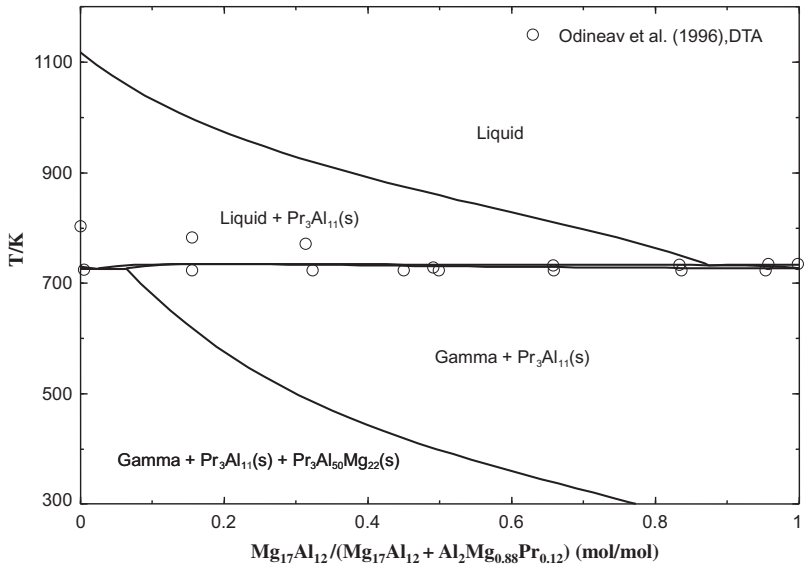

FIGURE 36. Calculated $Mg_{17}Al_{12}$–$Al_2Mg_{0.88}Pr_{0.12}$ section compared with experimental data of Odinaev *et al.* [35].

present study is closer to the temperature reported by Gröbner *et al.* [9]. Clearly, further experimental work to measure liquidus temperatures is required.

Figure 31 shows the calculated liquidus surface in the Mg–Al–Ce system. The liquidus surface is dominated by the Laves_C15 (almost pure Al_2Ce) and $Al_{11}Ce_3$ phases, which have high melting temperatures and very negative enthalpies of formations. The primary phase regions of these phases intersect that of Mg(HCP_A3). Therefore, these phases are likely to precipitate in the HCP phase during Mg alloy production. The peritectic-formed ternary phase $Al_{13}Mg_6Ce$ is in agreement with our experiment (figure 4).

In general, the thermodynamic calculation results in the present study give very similar or superior results when compared to the calculations by Gröbner *et al.* [9].

4.2.3. The Al–Mg–Pr system

The Gibbs energy of the liquid phase was calculated using the symmetric Kohler-like approximation [45] with no ternary interaction parameters for the liquid phase. The invariant reactions for the Al–Mg–Pr system are listed in table 9. The optimized model parameters for the solid solutions are summarized in tables 5–7.

For $Pr(Mg,Al)_{12}$, the similarity among the La, Ce, Pr and Nd was considered although no data for the solid solubility of Al in $PrMg_{12}$ phase were reported. The enthalpy of formation of $PrAl_{12}$ compound was calculated by the Miedema model in the present study. Similar to the Al–Mg–La and Al–Mg–Ce systems, thirteen ternary solid solutions (Laves_C15, BCC_B2, $(Mg, Pr)(Mg, Al)_3$, $Pr(Mg, Al)_3$, $Pr_3(Mg, Al)_{11}$, $Pr(Mg, Al)_{12}$, $(Mg, Al)_{41}Pr_5$, $(Mg, Al)_{17}Pr_2$,HCP_A3, FCC_A1, BCC_A2, DHCP_A3' and Gamma) were considered in the present study (table 1). For the Laves_C15 phase, two optimized interaction parameters for the first sub-lattice were required in order to reproduce the observed miscibility gap by Odinaev *et al.* [23] at $T = 673$ K. One interaction parameter was necessary to reproduce the 2-phase equilibria between the BCC_B2 and the DHCP_A3' (Pr) phases. For the $Pr(Al,Mg)_{12}$ phase, the Gibbs energy of hypothetical $PrAl_{12}$ and one interaction parameter were optimized in order to reproduce our experimental data. The ternary compound,

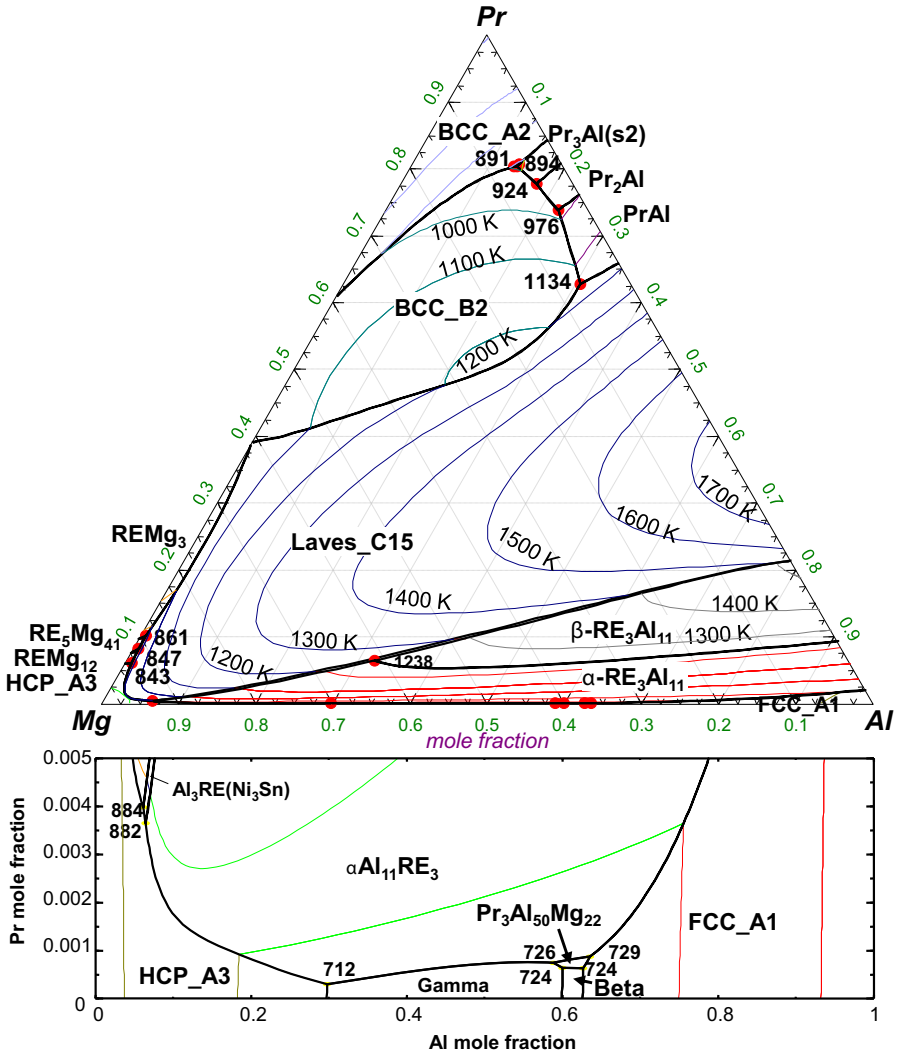

FIGURE 37. The liquidus projection of the Al–Mg–Pr system.

TABLE 10
Invariant reactions of the Al–Mg–Nd system for $X_{Nd} < 1/3$.

Reaction	T/K		Type[a]	Composition/(at.%)			
	Exp.[b]	Calc.		Phase	Calc.		
					Al	Nd	Mg
L ↔ Laves_C15 + Nd_5Mg_{41} + HCP_A3		820	E	L	0.6	7.4	92.0
L + Mg_3Nd ↔ Laves_C15 + Nd_5Mg_{41}		833	U	L	0.5	9.1	90.4
L + Al_3Nd ↔ HCP_A3 + $Al_{11}Nd_3$		845	U	L	11.9	0.3	87.8
L ↔ Gamma + Beta + $Nd_3Al_{50}Mg_{22}$	708	724	E	L	62.63	0.07	37.3
L ↔ Gamma + HCP_A3 + $Al_{11}Nd_3$	708	712	E	L	29.81	0.05	70.14
L ↔ Beta + Gamma + $Nd_3Al_{50}Mg_{22}$	709	724	E	L	59.98	0.07	39.95
L + $Al_{11}Nd_3$ + FCC_A1 ↔ $Nd_3Al_{50}Mg_{22}$		734	U	L	64.43	0.13	35.44

[a] P: peritectic, U: quasiperitectic, E: eutectic.
[b] Experimental data were taken from Odinaev *et al.* [38] unless another reference is given.

$Al_{50}Mg_{22}Pr_3$ (noted as $Al_2Mg_{0.88}Pr_{0.12}$ in [34]), was assumed to be a stoichiometric (line) compound in the present study because no solid solubility has been reported. The Gibbs energy of the $Al_{50}Mg_{22}Pr_3$ compound was optimized to reproduce phase equilibria at 673 K.

The calculated isothermal section of the Mg–Al–Pr ternary system at $T = 673$ K is shown in figure 32 along with the experimental data of Odinaev *et al.* [34]. PrMg and PrAl are only partially miscible because they have different crystal structures (CsCl and AlEr type, respectively). On the other hand, both $PrMg_2$ and $PrAl_2$ have the Cu_2Mg type structure and they form a Laves_C15 solid solution with a miscibility gap at low temperature. Most experimental data are well reproduced by the calculations. According to Odinaev *et al.* [34], $PrMg_2$ is stable and forms a solid solution at 673 K. However, this contradicts the result of Saccone *et al.* [76] who reported that $PrMg_2$ decomposes into $PrMg_3$ and PrMg near $T = 943$ K. $PrMg_2$ is only stable over a limited temperature range (943 K ~ 1013 K). However, it is stabilized over a wide temperature range as $PrAl_2$

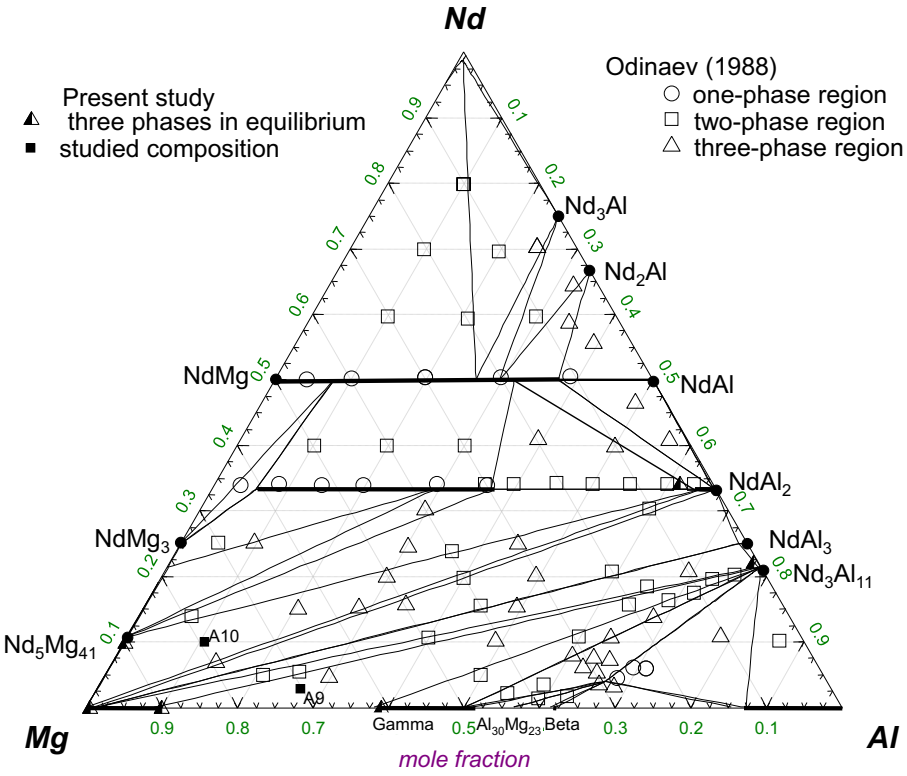

FIGURE 38. The calculated isothermal section of the Mg–Al–Nd ternary system at $T = 673$ K compared with experimental data of Odinaev *et al.* [37].

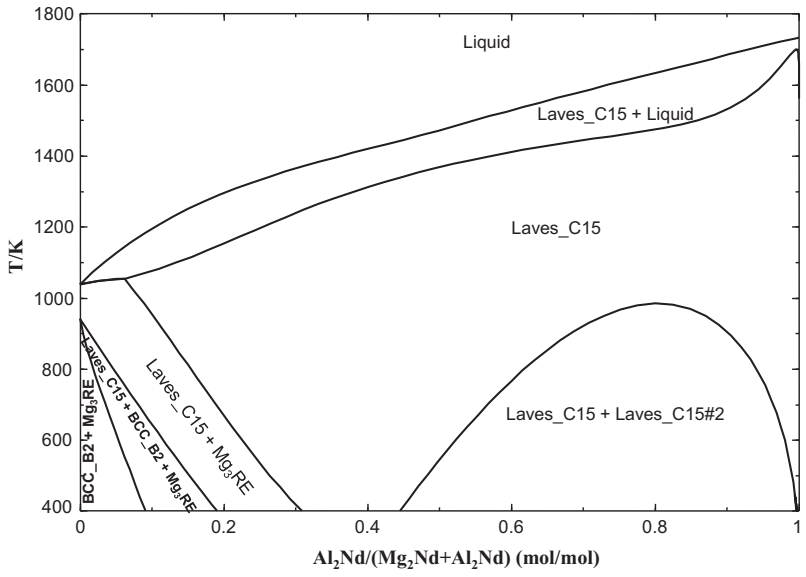

FIGURE 39. Calculated Al_2Nd–Mg_2Nd section.

dissolves into it. The miscibility gap in the Laves_C15 solution measured by Odinaev *et al.* [34] compares favourably with the present thermodynamic calculation.

Figures 33–36 show several calculated sections compared with the experimental DTA data by Odinaev *et al.* [35]. In all these figures, it can be observed that the thermodynamic calculations reproduce the temperatures where liquid alloys first form, through either eutectic or peritectic reactions, very closely. However, the reported liquidus temperatures of Odinaev *et al.* [34] are far below the present calculations. Similar discrepancies were also observed in calculations of the Mg–Al–La and Mg–Al–Ce system in the present study, in which experimental DTA data are also available from the work of Odinaev *et al.* [23,31]. It might be in error due to experimental difficulties at high temperature, although the experimental details were not given.

Figure 37 shows the calculated liquidus surface for the Al–Mg–Pr system. The liquidus surface is dominated by the Laves_C15 (almost pure Al_2Pr) and $Al_{11}Pr_3$ phases, which have high melting temperatures and very negative enthalpies of formations. The primary phase regions of these phases intersect that of Mg(HCP_A3). Therefore,

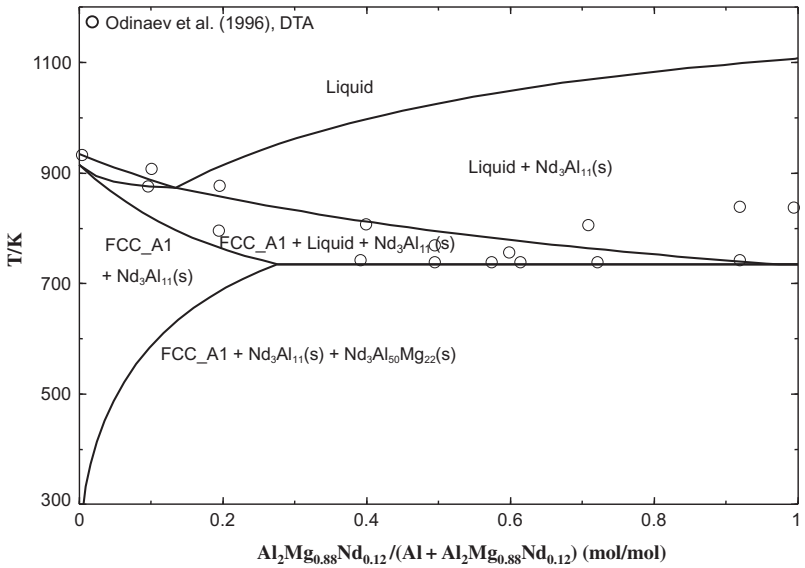

FIGURE 40. Calculated Al–$Al_2Mg_{0.88}Nd_{0.12}$ section compared with experimental data of Odinaev *et al.* [38].

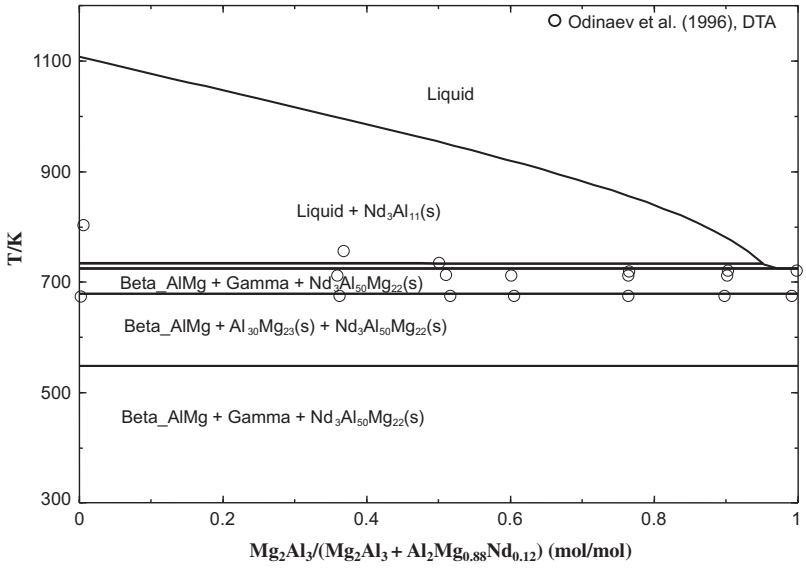

FIGURE 41. Calculated Mg_2Al_3–$Al_2Mg_{0.88}Nd_{0.12}$ section compared with experimental data of Odinaev *et al.* [38].

these phases are likely to precipitate in the HCP phase during Mg alloy solidification process. The peritectically formed ternary phase $Al_{50}Mg_{22}Pr_3$ is confirmed by our experiment (see figure 8).

4.2.4. The Al–Mg–Nd system

The invariant reactions for the Al–Mg–Nd system are listed in table 10. The Gibbs energy of the liquid phase was calculated using the symmetric Kohler-like approximation[45] with no ternary interaction parameters. The optimized model parameters are summarized in tables 5–7.

For $Nd(Mg,Al)_{12}$, the similarity among the La, Ce, Pr and Nd was considered although no data for the solid solubility of Al in $NdMg_{12}$ phase were reported. The enthalpy of formation of $NdAl_{12}$ compound was calculated via the Miedema model. Similar to the Al–Mg–La, Al–Mg–Ce and Al–Mg–Pr systems, thirteen ternary solid solutions (Laves_C15, BCC_B2, $(Mg, Nd)(Mg, Al)_3$,$Nd(Mg, Al)_3$, $Nd_3(Mg, Al)_{11}$, $Nd(Mg, Al)_{12}$, $(Mg, Al)_{41}Nd_5$, $(Mg, Al)_{17}Nd_2$,HCP_A3, FCC_A1, BCC_A2, DHCP_A3' and Gamma) were considered in the present study. For the Laves_C15 phase, like the Al–Mg–Pr system, two optimized interaction parameters for the first sub-lattice were required in order to reproduce the observed miscibility gap at $T = 673$ K by Odinaev *et al.* [37]. One interaction parameter was necessary to reproduce the 2-phase equilibria between the BCC_B2 and the DHCP_A3' (Nd) phases. The ternary compound, $Al_{50}Mg_{22}Nd_3$ (noted as $Al_2Mg_{0.88}Nd_{0.12}$ in [37]), was assumed to be a stoichiometric (line) compound in the present study because no solid solubility has been reported. The Gibbs energy of the $Al_{50}Mg_{22}Nd_3$ compound was optimized to reproduce phase equilibria at 673 K. In general, the optimization was directed mainly towards reproducing the phase equilibrium data at 673 K measured by Odinaev *et al.* [37].

A calculated isothermal section of the Mg–Al–Nd ternary system at $T = 673$ K is shown in figure 38 along with the experimental results of Odinaev *et al.* [37]. NdMg and NdAl are only partially miscible because they have different crystal structures (CsCl and AlEr type, respectively). On the other hand, both $NdMg_2$ and $NdAl_2$

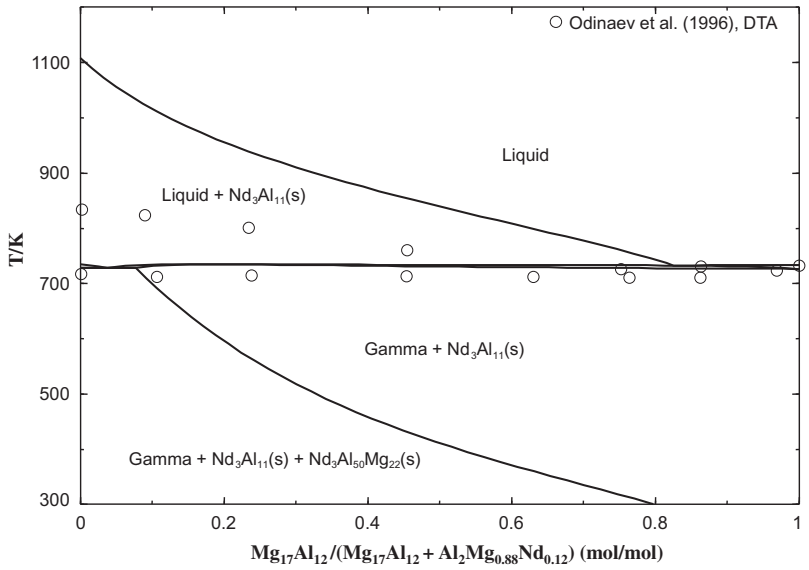

FIGURE 42. Calculated $Mg_{17}Al_{12}$–$Al_2Mg_{0.88}Nd_{0.12}$ section compared with experimental data of Odinaev *et al.* [38].

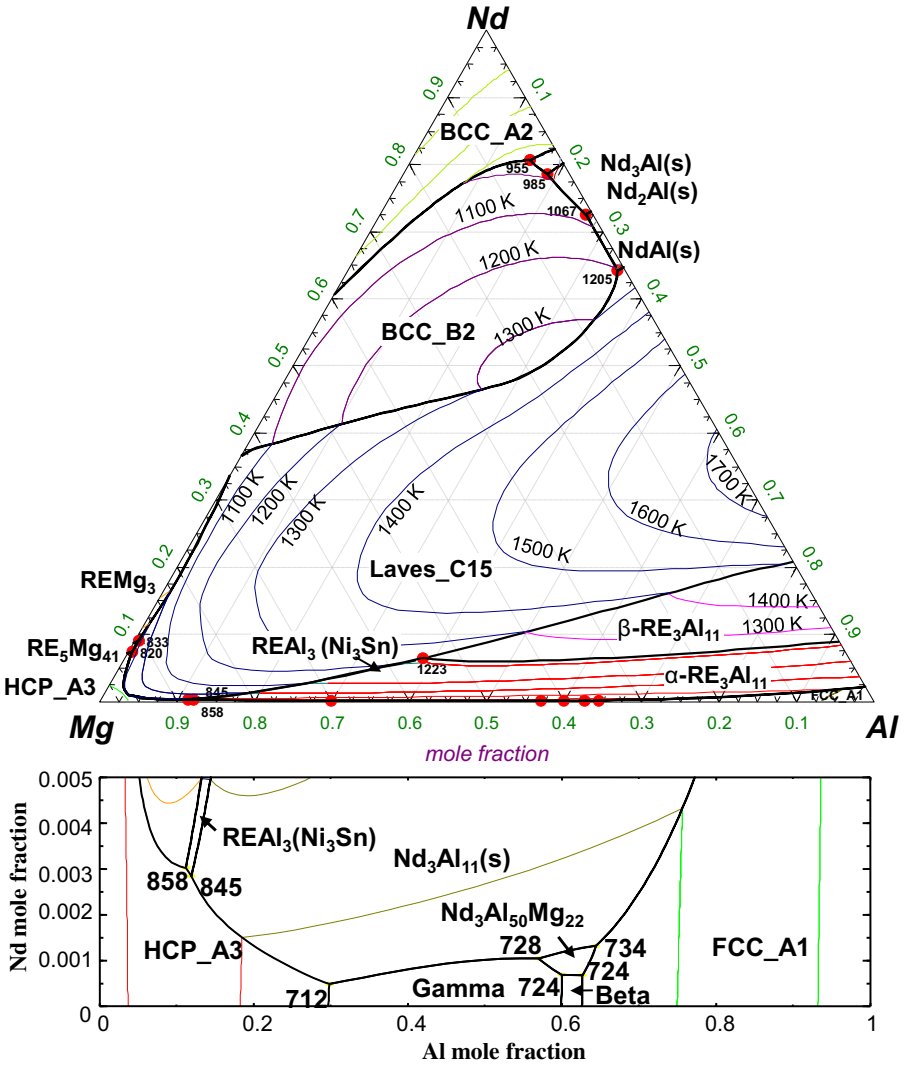

FIGURE 43. The liquidus projection of the Al–Mg–Nd system.

have the Cu_2Mg type structure and they form a Laves_C15 solid solution with a miscibility gap at low temperature. Most experimental data are well reproduced by the calculations. According to Odinaev *et al.* [37], $NdMg_2$ is stable and forms a solid solution at 673 K. However, this contradicts the result of Delfino *et al.* [77] who reported that $NdMg_2$ decomposes into $NdMg_3$ and NdMg near $T = 949$ K. $NdMg_2$ is only stable over a limited temperature range (949 K $\sim$ 1034 K). However, it is stabilized over a wide temperature range as $NdAl_2$ dissolves into it. The miscibility gap in the Laves_C15 solution measured by Odinaev *et al.* [37] compares favourably with the present thermodynamic calculations.

Figures 39–42 show several calculated sections compared with the experimental DTA data by Odinaev *et al.* [38]. In all these figures, it can be observed that the thermodynamic calculations reproduce the temperatures very closely, where liquid alloys first form, through either eutectic or peritectic reactions. However, the liquidus temperatures reported by Odinaev *et al.* [24] lie far below the present calculations. Similar discrepancies were also observed in calculations of the Mg–Al–La, Mg–Al–Ce and Mg–Al–Pr systems. It might be in error due to experimental difficulties at high temperature, although the experimental details were not given.

Figure 43 shows the calculated liquidus surface of the Mg–Al–Nd system. The liquidus surface is dominated by the Laves_C15 (almost pure Al_2Nd) and $Al_{11}Nd_3$ phases, which have high melting temperatures and very negative enthalpies of formations. The primary phase regions of these phases intersect that of Mg(HCP_A3). Therefore, these phases are likely to precipitate in the HCP phase during Mg alloy solidification process.

4.2.5. The Al–Mg–Sm system

The calculated isothermal section is illustrated in figure 44 with the experimental data at $T = 673$ K by Zheng *et al.* [40]. It was noted that intermetallic compound phases Al_4Sm and $AlSm_3$ have not been taken into consideration in this work. According to the recently assessed Al–Sm [15] binary phase diagram, there is an $Al_{11}Sm_3$ phase instead of Al_4Sm and no $AlSm_3$ phase. Moreover, Mg_5Sm and $Mg_{41}Sm_5$ exist in the Mg–Sm [16] binary phase diagram recently optimized, which were not taken into account by Zheng *et al.* [40]. Generally, the calculated isothermal section has reproduced the experimental data with satisfaction. It was worth noting a few differences in the optimization between Jia *et al.* [10] and the current study. First of all, there is a modification of Sm_3Al_{11} phase. In the present study, the Sm_3Al_{11} phase exists only at high-temperature range from 1351 K to 1684 K [15], which was mainly based on the investigation of Delsante *et al.* [78]. Secondly, the Mg_2Sm phase was considered to be stable at high-temperature range from 653 K to 1015 K [16] and decomposed to Mg_3Sm and MgSm phases at 653 K, which was similar to Mg_2La, Mg_2Ce, Mg_2Pr and Mg_2Nd phases. Thirdly, it was assumed that there is certain solid solubility of Al in MgSm (BCC_B2) phase, which was believed to be reasonable by considering the similarities among Al–Mg–La, Al–Mg–Ce, Al–Mg–Pr, Al–Mg–Nd, Al–Mg–Gd, Al–Mg–Dy, Al–Mg–Ho, Al–Mg–Er [13] and Al–Mg–Sm systems. Thirdly, it was believed that Mg_2Sm and Al_2Sm could form Laves_C15 solid solution since both of them have the same crystal structure (C15, $MgCu_2$-type). Finally, unlike the investigation of Zheng *et al.* [40], Al_4Sm and $AlSm_3$ were not considered in Al–Sm and Al–Mg–Sm systems; $Mg_{13}Sm_2$ was described as $Mg_{41}Sm_5$ and Mg_5Sm exists in Mg–Sm and Al–Mg–Sm systems [39], Al_3Mg_2 phase was considered as $Al_{30}Mg_{23}$. The Gibbs energy of the liquid phase was calculated using the symmetric Kohler-like approximation with no ternary interaction parameters.

For the Laves_C15 and BCC_B2 phases, the excess Gibbs energies were similar to the ones in Al–Mg–Pr and Al–Mg–Nd systems.

The liquidus projection with the univariant points was presented in figure 45. The liquidus surface is dominated by the Laves_C15 (almost pure Al_2Sm) and Ni_3Sn (Al_3Sm) phases, which have high melting temperatures and negative enthalpies of formations. The primary phase regions of these phases intersect that of

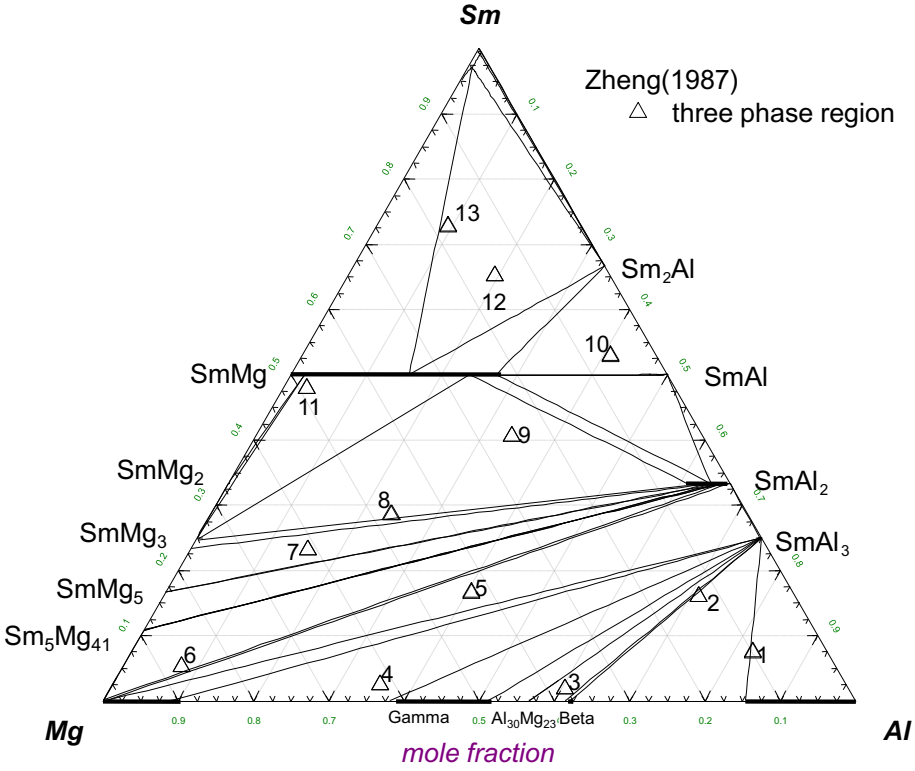

FIGURE 44. The calculated isothermal section of the Mg–Al–Sm ternary system at $T = 673$ K compared with experimental data of Zheng *et al.* [40].

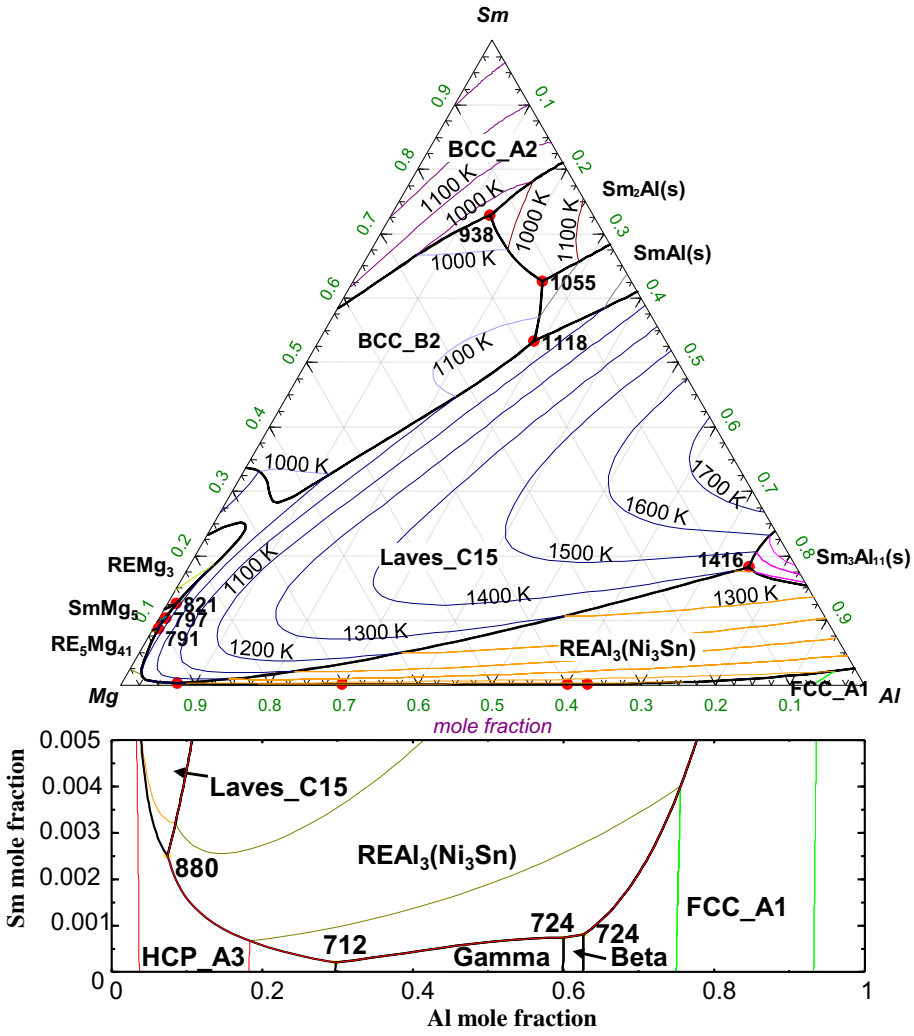

FIGURE 45. The liquidus projection of the Al–Mg–Sm system.

Mg(HCP_A3). Therefore, these phases are likely to precipitate in the HCP phase during Mg alloy solidification process.

The calculated invariant reactions in the Al–Mg–Sm system are listed in table 11 compared with the calculated results from Jia *et al.* [10]. The optimized model parameters are summarized in tables 5–7.

Compared to Al–Mg–La, Al–Mg–Ce, Al–Mg–Pr and Al–Mg–Nd systems, the Al–Mg–Sm system exhibits three dissimilarities. Firstly, no ternary compound was reported for the Al–Mg–Sm system, while one ternary compound with similar composition in the Al-rich part was reported for the Al–Mg–La, Al–Mg–Ce, Al–Mg–Pr and Al–Mg–Nd systems. It is worth noting that Sm (rhombohedral) has a different structure from La, Ce, Pr and Nd elements, all of which have a double hexagonal close-packed structure at low temperature. Secondly, there was almost no solid solubility of Mg in Laves_C15 (almost pure Al_2Sm) phase, contrary to Al–Mg–La, Al–Mg–Ce, Al–Mg–Pr and Al–Mg–Nd systems, where a miscibility gap would occur in Laves_C15 phase at low temperature (< 800 K). Although the topology of the Al–Mg–Sm isothermal section at $T = 673$ K is different between the present study and Jia *et al.* [10], there is no contradiction to the reported three-phase equilibria of Zheng *et al.* [40] for the alloys labelled as 8 and 9 in figure 44. Finally, Sm_3Al_{11} exists only at high temperature, different from La_3Al_{11}, Ce_3Al_{11}, Pr_3Al_{11} and Nd_3Al_{11}, which are stable down to room temperature.

Generally, the calculated isothermal section at $T = 673$ K shows satisfactory agreement with the experimental data of Zheng *et al.* [40].

5. Conclusions

Thermodynamic evaluations and optimizations of the Al–Mg–La, Ce, Pr, Nd, Sm systems have been systematically carried out on the basis of the literature information and new experimental results from this work. The Al–Mg–Pr and Al–Mg–Nd systems were optimized for the first time using a systematic approach. Similar model parameters were used for these five ternary systems. It was pointed out that previous thermal analysis data interpreted as liquidus temperature by Odinaev *et al.* [24,31,35,38] are much lower than the experimental data from [8,9] which is preferred in the present study. The Miedema model was used to calculate enthalpies of formation for the ternary compounds and metastable phases $Al_{12}RE$ ($Mg_{12}Ce$-oI338), $Al_{17}RE_2$ ($Ni_{17}Th_2$-hP38), and $Al_{41}RE_5$ ($Mg_{41}Ce_5$-tI92). The entropies of formation of these metastable phases are interpolated between Al and stable $Al_{11}RE_3$ phases. The difference of enthalpy of formation for Mg_3RE phase between two different structures (metastable Ni_3Sn-hP8 and stable BiF_3-cF16) are assumed to be the same as the those from first-principles by Tao *et al.* [64]. The calculated phase equilibria in the designated

TABLE 11
Some invariant reactions of the Al–Mg–Sm system for $X_{Sm} < 1/3$.

Reaction	T/K		Type[a]	Composition/(at.%)			
	Exp.	Calc.		Phase	Calc.		
					Al	Sm	Mg
L ↔ Laves_C15 + Sm_5Mg_{41} + HCP_A3		791	E	L	0.6	8.8	90.6
L + $SmMg_5$ ↔ Laves_C15 + Sm_5Mg_{41}		797	E	L	0.8	10.4	88.8
L + Mg_3Sm ↔ Laves_C15 + $SmMg_5$		821	U	L	1.2	12.6	86.2
L + $Al_{11}Sm_3$ + Laves_C15 ↔ Al_3Sm		1416	P	L	75.3	18.3	6.4
L ↔ HCP_A3 + Gamma + Al_3Sm		712	E	L	29.78	0.02	70.2
L + FCC ↔ Beta + Al_3Sm		724	U	L	62.68	0.08	37.24
L + Beta ↔ Gamma + Al_3Sm		724	U	L	59.99	0.07	39.94
L ↔ HCP_A3 + Laves_C15 + Al_3Sm		880	E	L	7.4	0.3	92.3

[a] P: peritectic, U: quasiperitectic, E: eutectic.

equilibrated-alloys agree well with the experiments carried out in the present investigation. The optimized phase diagrams agreed well with our key experiments. No ternary parameters were used for the liquid in ternary systems. The extrapolation from the binary systems produced a satisfactory agreement with the ternary experimental data, thus indicating well described Gibbs energy data sets of the binary phases.

Acknowledgements

Financial supports from General Motors of Canada Ltd. and the Natural Sciences and Engineering Research Council of Canada through the CRD grant program are gratefully acknowledged. One of the authors, Ms Jin, would like to express her gratitude to REGAL and FQRNT for their financial support of this project. The authors would like to thank Dr. Shi in McGill University for the technical assistance on the experiment work.

References

[1] Z. Yang, J.P. Li, J.X. Zhang, G.W. Lorimer, J. Robson, Acta Metall. Sin. (Engl. Lett.) 21 (2008) 313–328.
[2] J. Gröbner, R. Schmid-Fetzer, Scr. Mater. 63 (2010) 674–679.
[3] G. Pettersen, H. Westengen, R. Hoier, O. Lohne, Mater. Sci. Eng. A 207 (1996) 115–120.
[4] K. Hantzsche, J. Bohlen, J. Wendt, K.U. Kainer, S.B. Yi, D. Letzig, Scr. Mater. 63 (2010) 725–730.
[5] S. Yi, J. Bohlen, F. Heinemann, D. Letzig, Acta Mater. 58 (2010) 592–605.
[6] G. Cacciamani, S. De Negri, A. Saccone, R. Ferro, Intermetallics 11 (2003) 1135–1151.
[7] G. Cacciamani, A. Saccone, S. De Negri, R. Ferro, J. Phase Equilib. 23 (2002) 38–50.
[8] M. Hosseinifar, D.V. Malakhov, J. Alloys Compd. 505 (2010) 459–466.
[9] J. Gröbner, D. Kevorkov, R. Schmid-Fetzer, Intermetallics 10 (2002) 415–422.
[10] B.R. Jia, L.B. Liu, D.Q. Yi, Z.P. Jin, J.F. Nie, J. Alloys Compd. 459 (2008) 267–273.
[11] S. De Negri, A. Saccone, G. Cacciamani, R. Ferro, Intermetallics 11 (2003) 1125–1134.
[12] A. Saccone, G. Cacciamani, S. De Negri, R. Ferro, J. Phase Equilib. 23 (2002) 29–37.
[13] L. Jin, Thermodynamic modelling of aluminum–magnesium–rare earth systems (Ph.D. thesis), Chemical engineering, Ecole polytechnique de Montréal, Montréal, 2012.
[14] P. Chartrand, École Polytechnique de Montréal, Canada, 2006, unpublished research.
[15] L.-L. Jin, Y.-B. Kang, P. Chartrand, C.D. Fuerst, Calphad 35 (2011) 30–41.
[16] Y.-B. Kang, L. Jin, P. Chartrand, A.E. Gheribi, K. Bai, P. Wu, Calphad 38 (2012) 100–116.
[17] Y.-B. Kang, A.D. Pelton, P. Chartrand, C.D. Fuerst, Calphad 32 (2008) 413–422.
[18] L.-L. Jin, P. Chartrand, Y.-B. Kang, C.D. Fuerst, Calphad 34 (2010) 456–466.
[19] Y.-B. Kang, École polytechnique de Montréal, Canada, 2008, unpublished work.
[20] P. Rogl, Ternary alloys: a comprehensive compendium of evaluated constitutional data and phase diagrams, in: G. Petzow, G. Effenberg, (Eds.), Weinheim, New York, 1988.
[21] V. Raghavan, J. Phase Equilib. Diffus. 29 (2008) 270–271.
[22] O.S. Zarechnyuk, V.V. Kinzhibalo, A.T. Tyvanchuk, R.M. Rykhal, Izvestiya Akademii Nauk SSSR, Metally (1981) 221–223.
[23] K.O. Odinaev, I.N. Ganiev, V.V. Kinzhibalo, A.T. Tyvanchuk, Izv. Vyssh. Uchebn. Zaved., Tsvetn. Metall. (1988) 81–85.
[24] K.O. Odinaev, I.N. Ganiev, Metally (1995) 161–166.
[25] C. Guo, Z. Du, J. Alloys Compd. 385 (2004) 109–113.
[26] B. Darriet, M. Pezat, A. Hbika, P. Hagenmuller, Mater. Res. Bull. 14 (1979) 377–385.
[27] C. Zheng, Y. Xing, J. Qian, Y. Ye, Jinshu Xuebao 19 (1983) A515–A520.
[28] K.O. Odinaev, I.N. Ganiev, V.V. Kinzhibalo, K.K. Kurbanov, Izv. Vyssh. Uchebn. Zaved., Tsvetn. Metall. (1989) 75–77.
[29] O.S. Zarechnyuk, P.I. Kripyakevich, Izvestiya Akademii Nauk SSSR, Metally (1967) 188–190.
[30] Z. Cui, R. Wu, Jinshu Xuebao 20 (1984) B323–B331.
[31] K.O. Odinaev, I.N. Ganiev, A.Z. Ikromov, Metally (1996) 165–169.
[32] C. Zheng, Y. Wu, J. Qian, Y. Ye, Jinshu Xuebao 22 (1986) B63–B67.
[33] V. Raghavan, J. Phase Equilib. Diffus. 29 (2008) 275–277.
[34] K.O. Odinaev, I.N. Ganiev, V.V. Kinzhibalo, Izv. Vyssh. Uchebn. Zaved., Tsvetn. Metall. (1988) 91–94.
[35] K.O. Odinaev, I.N. Ganiev, A.Z. Ikromov, Metally (1996) 170–173.
[36] V. Raghavan, J. Phase Equilib. Diffus. 29 (2008) 272–274.
[37] K.O. Odinaev, I.N. Ganiev, V.V. Kinzhibalo, A.T. Tyvanchuk, Izv. Vyssh. Uchebn. Zaved., Tsvetn. Metall. (1988) 94–97.
[38] K.O. Odinaev, I.N. Ganiev, A.Z. Ikromov, Metally (1996) 168–172.
[39] V. Raghavan, J. Phase Equilib. Diffus. 30 (2009) 69–70.
[40] C. Zheng, L. Chen, Y. Ye, Jinshu Xuebao 23 (1987) B117–B120.
[41] F.R.D. Boer, R. Boom, W.C.M. Mattens, A.R. Miedema, A.K. Niessen, Cohesion in Metals: Transition Metal Alloys, North-Holland, New York, 1988.
[42] H. Bakker, Enthalpies in alloys. Miedema's semi-empirical model, Enfield Publishing & Distribution Company, 1998.
[43] S.P. Sun, D.Q. Yi, H.Q. Liu, B. Zang, Y. Jiang, J. Alloys Compd. 506 (2010) 377–387.
[44] J. Basu, B.S. Murty, S. Ranganathan, J. Alloys Compd. 465 (2008) 163–172.
[45] A.D. Pelton, Calphad 25 (2001) 319–328.
[46] A.B. Shubin, K.Y. Shunyaev, Rasplavy (2010) 44–50.
[47] C.W. Bale, P. Chartrand, S.A. Degterov, G. Eriksson, K. Hack, R. Ben Mahfoud, J. Melancon, A.D. Pelton, S. Petersen, Calphad 26 (2002) 189–228.
[48] A.T. Dinsdale, Calphad 15 (1991) 317–425.
[49] A.D. Pelton, S.A. Degterov, G. Eriksson, C. Robelin, Y. Dessureault, Metall. Mater. Trans. B 31B (2000) 651–659.
[50] Y.-B. Kang, A.D. Pelton, P. Chartrand, P. Spencer, C.D. Fuerst, Metall. Mater. Trans. A 38 (2007) 1231–1243.
[51] Y.-B. Kang, A.D. Pelton, P. Chartrand, P. Spencer, C.D. Fuerst, J. Phase Equilib. Diffus. 28 (2007) 342–354.
[52] Y.-B. Kang, I.-H. Jung, S.A. Decterov, A.D. Pelton, H.-G. Lee, ISIJ Int. 44 (2004) 975–983.
[53] I.-H. Jung, S.A. Decterov, A.D. Pelton, J. Eur. Ceram. Soc. 25 (2005) 313–333.
[54] A. Pelton, P. Chartrand, Metall. Mater. Trans. A 32 (2001) 1361–1383.
[55] P. Chartrand, A. Pelton, Metall. Mater. Trans. A 32 (2001) 1385–1396.
[56] P. Waldner, A.D. Pelton, Metall. Mater. Trans. B 35B (2004) 897–907.
[57] M. Hillert, L.-I. Staffansson, Acta Chem. Scand. 24 (1970) 3618–3626.
[58] H. Harvig, Acta Chem. Scand. 25 (1971) 3199–3204.
[59] B. Sundman, J. Ågren, J. Phys. Chem. Solids 42 (1981) 297–301.
[60] J.-O. Andersson, A.F. Guillermet, M. Hillert, B. Jansson, B. Sundman, Acta Metall. 34 (1986) 437–445.
[61] A. Saccone, D. Macciò, J.A.J. Robinson, F.H. Hayes, R. Ferro, J. Alloys Compd. 317–318 (2001) 497–502.
[62] M.C. Gao, A.D. Rollett, M. Widom, Phys. Rev. B: Condens. Matter Mater. Phys. 75 (2007) 174120/174121–174120/174116.
[63] X. Tao, First-principles calculations on the thermodynamic properties of Al-Rare Earth and Mg-Rare Earth alloys, materials science, Central South University, Changsha, China, 2008. pp. 133.
[64] X. Tao, Y. Ouyang, H. Liu, Y. Feng, Y. Du, Y. He, Z. Jin, J. Alloys Compd. 509 (2011) 6899–6907.
[65] R.H. Taylor, S. Curtarolo, G.L.W. Hart, Phys. Rev. B 84 (2011) 084101.
[66] S. Curtarolo, W. Setyawan, S. Wang, J. Xue, K. Yang, R.H. Taylor, L.J. Nelson, G.L.W. Hart, S. Sanvito, M. Buongiorno-Nardelli, N. Mingo, O. Levy, Comp. Mater. Sci. 58 (2012) 227–235.

[67] I. Ansara, A.T. Dinsdale, M.H. Rand (Eds.), COST 507: Thermochemical Database for Light Metal Alloys, Luxembourg, 1998.
[68] P. Liang, H.-L. Su, P. Donnadieu, M.G. Harmelin, A. Quivy, P. Ochin, G. Effenberg, H.J. Seifert, H.L. Lukas, F. Aldinger, Z. Metallkd. 89 (1998) 536–540.
[69] S.H. Zhou, R.E. Napolitano, Acta Mater. 54 (2006) 831–840.
[70] M. Giovannini, A. Saccone, R. Marazza, R. Ferro, Metall. Mater. Trans. A 26 (1995) 5–10.
[71] R.V. Denys, A.A. Poletaev, J.K. Solberg, B.P. Tarasov, V.A. Yartys, Acta Mater. 58 (2010) 2510–2519.
[72] A.A. Poletaev, R.V. Denys, J.K. Solberg, B.P. Tarasov, V.A. Yartys, J. Alloys Compd. 509 (Suppl. 2) (2011) S633–S639.
[73] R. Vogel, T. Heumann, Z. Metallkd. 38 (1947) 1–8.
[74] K.A. Gschneidner, V.K. Pecharsky, J. Cho, S.W. Martin, Scr. Mater. 34 (1996) 1717–1722.
[75] K.O. Odinaev, I.N. Ganiev, Izv. Vyssh. Uchebn. Zaved., Tsvetn. Metall. (1990) 90–95.
[76] A. Saccone, A.M. Cardinale, S. Delfino, R. Ferro, Intermetallics 1 (1993) 151–158.
[77] S. Delfino, A. Saccone, R. Ferro, Metall. Trans. A 21A (1990) 2109–2114.
[78] S. Delsante, R. Raggio, G. Borzone, R. Ferro, J. Phase Equilib. Diffus. 28 (2007) 240–242.

JCT 12-426